# Investigating Upwelled Water Over Spur Canyon

Rob Irwin

June 22, 2015

# Contents

# List of Tables

# List of Figures

# Chapter 1

# Literature Review and Problem Definition

## 1.1 Description of the Juan de Fuca Eddy

The eddy is a cyclonic feature located off the entrance to Juan de Fuca strait. It is seen in the summer as a consequence of northwesterly wind stress producing a southeastward current. This southeastward current produces upwelling conditions along the coast of Southern Vancouver Island. This upwelled water transports deeper nutrient rich water to the shelf, and plays a significant role in increasing biological productivity in this region of the northeast Pacific.

This eddy was first proposed by [Tully, 1941]. In [Freeland and Denman, 1982] , the authors proposed that the eddy appears during the "spring transition" when prevailing alongshore winds switch from southeasterly to northwesterly and drive a southeastward current over the outer continental shelf and slop (direct quote from [Foreman et al., 2008]). The upper layer of the eddy is reportedly in geostrophic (or very near geostrophic) balance – the outward Coriolis force is balanced by the inward pressure gradient. Regionally, the Spur (or Tully) Canyon blocks mid-depth flow and disrupts this momentum balance. This blocking has the effect of reducing flow velocity,

and thus Coriolis force. This causes an imbalance because the inward pressure force remains, forcing an "up-canyon" current to form.

In [Freeland and Denman, 1982], the water of the Juan de Fuca eddy was shown to be composed of California Undercurrent water. It was this deep water that was upwelled onto the shelf that formed the eddy. However, [Foreman et al., 2008] suggest that "the denser water that is upwelled to form the eddy is not solely composed of California Undercurrent water". They suggest this because of studies of water composition in Juan de Fuca canyon showing that California Undercurrent water and coastal deep waters are present.

## 1.2  Literature Review

### 1.2.1  [Freeland and Denman, 1982]; A topographically controlled upwelling center off southern Vancouver Island

Observations from January 1979-June 1981 were performed to study the annual upwelling event seen off the coast of southern Vancouver Island. A motivation for this study was to determine whether oceanic regions adjacent to Vancouver Island belonged to the Alaska Gyre system, the California Current system, or neither. As stated in other studies, the summer winds in the area are "extremely favourable for upwelling" (citing two papers, [Bakun, 1975] and [Nelson, 1977]). The region of study is a line extending perpendicularly from Vancouver Island into the Pacific Ocean (figure 1 of article). The line does not intersect major regions of study in [Foreman et al., 2008], and the line is north of the Spur Canyon rim. Stated in the introduction: La Perouse Bank is the only topographic feature with a length scale larger than the internal Rossby radius of deformation and so it is the only one likely to be able to modify substantially the large scale geostrophic flows. Current meter moorings and CTD's were used to observe the study region. The dissolved oxygen content was measured over the study period. At station 105, a significant drop in dissolved oxygen is generally observed

around springtime and it is stated that "the spring decline in oxygen is much faster than can be accounted for by biological oxygen demand." The dissolved oxygen levels were seen to return back to a "normal" state in the fall. Upwelling indices are shown. The indices are calculated as weekly averages. Not surprisingly, at station 105 (along the shelfbreak roughly), the upwelling index is periodic in nature, with positive values in the summer, and negative values in the winter.

The first clear picture of the Juan de Fuca eddy is shown in figure 5, where a contour plot of $\sigma_t$, or potential density is shown at a fixed depth. The authors state that there is a definite "front" in the $\sigma_t$ field – the front appears to correspond with the depth of shelf-break in the region. A region of high $\sigma_t$ is seen to develop just north of Spur Canyon, indicating the centre of the eddy. It should be noted that the authors develop contour maps using the technique of "objective analysis" and cite Bretherton et al. [1976]. This is noted because the study area indicated was a perpendicular line, however the authors show area maps, well south of the line of interest.

Further in the text, the authors present a contour map of a variable, $\tau$. They describe $\tau$ as:

> ... a function of temperature and salinity that is orthogonal to $\sigma_t$ curves on a $T/S$ plot. Though the actual values are of no consequence it is a convenient measure of how different two water masses are that share the same $\sigma_t$ value. It is not affected by seasonal changes that might make density more or less strongly determined by salinity or temperature. If two water masses have the same $\tau$ on any given $\sigma_t$ surface, then those two water masses are identical.

This is effectively what is known as *spice*.

The authors then establish that during the summer months, at station 105, the water mass at $100m$ depth is evidently California Undercurrent water. They state:

> Somehow California Undercurrent water is being raised from depth and deposited on the continental shelf. The observations that this water is low

in oxygen and high in nutrients further confirm the notion that the water has been away from the surface layer for a considerable time. However, to date there have been no direct observations of the California Undercurrent this far north.

It is seen to be a curious case that water so deep was raised to the surface with non-standard upwelling conditions. There are four details specified by the authors that suggest this upwelling event is not of the classical kind, but rather a special locally determined phenomena:

1. upwelling is considered to be a local response to local winds, however the upwelling index combined with wind observations refute this

2. depths of classical upwelling are typically only moderate depths below the shelf-break — they cite $250m$ as the expected depth of upwelling, when in reality this event must take water from $450m$

3. the frequency of upwelling is expected to have the same frequency as that of the winds. Here, there is one long sustained event per year that lasts for longer than 100 days.

4. "There should be nothing particularly special about the response at this location". They state northern Vancouver Island sees the same wind forcing conditions, but annual cycles are much smaller magnitude than observed here.

Current meter observations along the observation line indicate directionality and magnitude of currents at depths of $50m$ and $100m$ (figure 8 of text). Currents these depths are typically towards the northwest during downwelling, and towards the south east during upwelling. Stations CZ4 (continental slope station) and CZ3 (shelf edge station) are discussed first. In terms of directionality, the authors concisely state that the currents are "strongly polarized parallel to the local bathymetry", with magnitudes around $20cm/s$ in the winter. A sharp transition occurs on March 18th 1980 at CZ3,

then four days later at CZ4, in terms of current directionality. This sharp transition has been dubbed "the spring transition". Authors note that although one might expect the winds and currents to be in phase, the major change in wind system occured on March $8^{th}$, considerably earlier. The following year, 1981, the wind transition occured on March $28^{th}$, while the current transition occured around March $6^{th}$. From the authors:

> The conclusion is, therefore, that the major seasonal cycles in currents are not strongly coupled to the local wind system.

For stations CZ1 and CZ2, there were some difficulties in the data, and much of the summer information was lost over the course of the study. Seasonality was still reported, however the data gives a much weaker seasonal dependence than the two more offshore stations.

Vertical shear is discussed in the following section, along with dynamic height (not summarized here).

The authors propose that because the eddy is "always closely associated with the northern terminus of the Spur Canyon", that the canyon is an essential component of this upwelling phenomena. They outline a sequence of events that leads to this upwelling behaviour:

1. in winter, shelf edge currents are northbound and the Juan de Fuca outflow current is also northbound along the coast

2. in ear spring (say mid-March) the shelf edge current reverses (the spring transition) and a cyclonic eddy is spun up on the wide continental shelf. Stratification is initially weak so vertical shear is initially small

3. the eddy is quasi-geostrophic and flows over the Spur Canyon; however, the canyon width is about half the internal Rossby radius of deformation, so the geostrophic circulation in the eddy cannot be significantly influenced by the presence of the canyon

4. since in the early spring vertical shear is small, water parcels moving in the eddy experience an inward pressure gradient that is largely balanced by an outward Coriolis force. Near the bottom these forces are still felt; however, inside the Spur Canyon water parcels experience only the pressure gradient force since the horizontal motion of water parcels is suppressed by the blocking effect of the Canyon

5. the inward pressure gradient forces a weak flow up the canyon to develop which advects water from the mouth of the canyon system onto the continental shelf

6. water originally in the canyon system at the time of the spring transition flows onto the continental shelf, and accounts for the slow decline in dissolved oxygen levels seen between the spring transition and the rapid decline in oxygen levels

7. as water originating from the California Undercurrent passing the mouth of the Juan de Fuca arrives on the shelf, we observe the rapid decline in oxygen values seen in early June of each year

8. as dense water accumulates on teh shelf horizontal density gradients increase, vertical shear increases (through the thermal wind relation) and the deep inward pressure gradient decreases. If water tends to flow back down the canyon the vertical shear will decrease which will tend to restore the inward pressure gradient

The following section attempts to prove that the classical model of wind-driven upwelling is insufficient for this specific case. It is shown that the volume of anomalous water on the shelf during summer months cannot be driven by classical upwelling. Following this proof, a toy model is created to show how deep water may be upwelled through a rectangular canyon. The depth of upwelling derived matches well with observations. However, this model neglects Coriolis forces and local effects. It is also a steady state model.

## 1.2.2   [Mackas et al., 1987]; Least Squares Multiple Tracer Analysis of Water Mass Composition

A mathematical formulation of water mass composition is put forth (not summarized here). Instead, the results of this mass composition analysis will be shown. The important information presented in this paper is contained within table 1, and figure 3.

| | Source | | | | |
|---|---|---|---|---|---|
| | Juan de Fuca | Offshore | Subarctic | California Under-current | Coastal Deep |
| Temperature, $°C$ | 9.84 | 8.75 | 4.70 | 6.90 | 5.10 |
| Salinity | 31.55 | 32.62 | 33.57 | 33.90 | 34.10 |
| Nitrate, $\mu$mol | 24.68 | 7.63 | 29.00 | 33.40 | 40.00 |
| Phosphate, $\mu$mol | 2.19 | 1.11 | 2.30 | 2.65 | 3.20 |
| Silicate, $\mu$mol | 41.76 | 12.55 | 48.00 | 52.00 | 90.00 |
| Oxygen, $mL/L^{-1}$ | 5.26 | 6.20 | 4.65 | 2.10 | 0.50 |

Table 1.1: Table 1 from [Mackas et al., 1987]

Five transects beginning along the coast and moving from towards the Pacific are considered in their paper. Line A transects the Washington Coast and heads directly west, offshore to the shelf break. Lines B-E begin along the coast of Vancouver Island and move south-west towards the shelf break. Line B is of primary importance to the present research, as it appears to cross a region near Spur Canyon. Each line will be analyzed for water composition based on table 1.1.

It is noted in the text that the middle of lines A and B are where the upwelling focus is concentrated.

- **Line A**

  Juan de Fuca water composes only a small part of the entire volume. It is confined to the top 50m and even when it is detectable, only accounts for half-or-less of the water volume.

Offshore water is more dominant away from the immediate coast, however it still composes 25-50% of the top 100m of coast water. Traces of offshore water are not apparent past 150m in depth, and most of its influence is contained in the top 100m of the water volume along this transect.

Subarctic water is not detectable along transect A.

The California Undercurrent accounts for a large portion of the water volume. In particular, the deeper water below 100m depth is > 75% composed of the California Undercurrent water mass. Each measured station showed that this water mass contributed for > 50% of the volume below 50m in depth. The shallower portions of the water volume show a significantly attenuated contribution from the undercurrent.

Coastal Deep water appears to be confined in a trench area along line A, however the contribution is small (< 25%).

- **Line B**

  Juan de Fuca water is a more significant contributer to the water composition of line B. The surface waters near the coast are largely sourced from the Juan de Fuca waters. Moving offshore, the contribution of JdF water decreases. There are two separated "blobs" of JdF water at depths of 75m and 120m, respectively, however it is unclear if this is error. Regardless, the contribution of these blobs is between 10% and 25%.

  Offshore water plays a larger role in the line B transect. As the shelf begins to break, the contribution of offshore water increases (not surprisingly). This contribution is still limited to the top 200m, even after the shelf break. On the shelf, the contribution is contained to the top 50m. There are small regions of high-contribution from offshore water, however the surface waters are not of primary interest here.

  Subarctic waters are seen offshore, past the shelf break, however its contribution

is small.

Once again, California Undercurrent waters dominate this line transect. In many ways, its contribution is similar to that of line A; the deeper waters are largely composed of CU water, and its contribution attenuates nearer to the surface. There are no traces of CU water for deeps shallower than 20m. The most prominant contribution

The most relevant part of their analysis is quoted here:

Results from other time periods (not presented here) confirmed [Freeland and Denman, 1982] interpretation that strong seasonal variations in the depth of isopycnal surfaces and in dissolved oxygen concentration are due to changes in the amount of upwelled Undercurrent water lying on the shelf. For example, near the middle of line B, the vertically averaged contribution from the two Undercurrent sources ranges from a winter low of about 5% of the water column to a summer high of over 70%. The difference between these two is a minimum estimate for the fraction of shelf water that is displaced (mostly within a time span of about 50 days [see [Freeland and Denman, 1982]]) by deep seasonal upwelling. The actual flushing rate is certainly higher, since some of the upwelled water is itself flushed from the shelf by subsequent upwelling.

The data source used for the line transects is summarized in:
Hill, S., K. Denman, D. Mackas, and H. Sefton, Ocean ecology data report: Coastal waters off southwest Vancouver Island, Spring and summer 1979, Can. Data Rep. Hydrog. Ocean Sci., 3, 118 pp., 1982a.
Hill, S., K. Denman, D. Mackas, and H. Sefton, Ocean ecology data report: Coastal waters off southwest Vancouver Island, Spring and summer 1980, Can. Data Rep. Hydrog. Ocean Sci., 4, 103 pp., 1982b.
Hill, S., K. Denman, D. Mackas, H. Sefton, and R. Forbes, Ocean ecology data report:

Coastal waters off southwest Vancouver Island, Spring and summer 1981, Can. Data Rep. Hydrog. Ocean Sci., 8, 93 pp., 1983.

## 1.2.3  [Meinvielle and Johnson, 2013]; Decadal water-property trends in the California Undercurrent, with implications for ocean acidification

The article begins with a good summary of the California Current System and the origins. The CCS consists of two parts; the California Current (CC) and the California Undercurrent (CU/CUC). The CC is described as a "shallow, narrow, meandering" current flowing southward, fed by the North Pacific Current. The North Pacific Current is classified as: cold, fresh, nutrient-poor, oxygen-rich, and relatively high-pH. The North Pacific Current is an eastward flowing oceanic current that reaches WCVI and forms the CC. The CUC is fed by Pacific equatorial water from the south, and is described as "warm, salty, nutrient-rich, oxygen-poor, and acidic."

In terms of seasonal variability, the CUC is strong during the summer when upwelling occurs. Surface southward jets become enhanced by strong winds and subsurface water gets upwelled onto the shelf (although this is not the direct cause of the strong upwelling). Upwelled water originates from 100-200m in depth, near the depth of the CUC core. This core depth is defined as the $\sigma_\theta = 26.6 kg \cdot m^{-3}$ surface by [Lynn and Simpson, 1987], but more recently as the $26.4 < \sigma_\theta < 26.5 kg \cdot m^{-3}$ surface by [Gay and Chereskin, 2009]. The approximate position of the CUC is estimated to be $20 - 25 km$ offshore of the shelf break.

Authors for this study use historical data from $1950 - 2012$ in the region to analyze how the CCS water composition changes over long periods. The coordinate system used is: isopycnals for the vertical coordinate, and bottom depth and latitude for horizontal coordinates. The use of bottom depth as a horizontal coordinate is justified by smoothing out multi-valued components of the coordinate; i.e. small scale features that do not follow the trend of monotonically increasing depth are not included.

## 1.2.4 [Foreman et al., 2008]; Modeling Juan de Fuca Eddy Generation

Authors use ROMS to investigate the formation of the reported Juan de Fuca eddy. Seven numerical experiments are considered, and are summarized in table 1 of their paper. This table is reproduced here in table 1.2.

| Exp. | Initial Conditions | Winds | Tides | Estuarine Flow | Objective |
|---|---|---|---|---|---|
| A | summer climatology | summer up-welling | yes | yes | baseline run |
| B | summer climatology | no | no | yes | to study the role of boundary nudging |
| C | identical profiles everywhere | summer up-welling | yes | no | to study the importance of the estuarine flow |
| D | summer climatology | summer up-welling | no | yes | to study the importance of upwelling favourable winds |
| E | summer climatology except off the entrance of the strait | summer up-welling | yes | yes | to study the importance of an eddy in the initial conditions |
| F | summer climatology | no | yes | yes | to study the role of tides |
| G | summer climatology | winter | yes | yes | to study the role of winter winds |

Table 1.2: Table taken from [Foreman et al., 2008] (table 1).

The experiments show that the Juan de Fuca eddy is generated with reasonable accuracy compared to several observational studies done in the area. As stated by the authors

> "... the Juan de Fuca eddy can be generated with average summer upwelling favourable winds, an average summer estuarine flow in the strait, and the

four major tidal constituents. Comparisons with analyzed current meter
and ADCP observations near the entrance to the strait demonstrated that
the model currents are reasonably accurate, thereby giving credibility to
the model dynamics and suggesting that the dynamics generating the eddy
in the model are real."

However, just because the eddy is generated with these four primary considerations,
the influence of each effect on the eddy was not explicitly shown. Hence, experiments
B-G explore the sensitivity of the eddy to each parameter.

For simulation B, the initial conditions were taken the same, but winds and tides
were turned off to investigate the role of boundary conditions in the model. The
boundary conditions used were "nudging" conditions, where boundary values would
slowly relax to climatological data. It should be noted that these boundary conditions
are only applied along the northern, southern and western parts of the model domain
(as the eastern boundary is determined by estuarine flow). In this simulation, a weak
eddy was seen (see figure 9) in the location of the Juan de Fuca eddy, however it
was much weaker than in simulation A and in observations. The authors suggested
that it was only present as a result of the initial conditions. They attribute the lack
of an eddy forming as a result of the lack of winds and tides. The general flow is
coastally constrained and towards the northwest, as opposed to simulation A which
established an offshore southeast directed flow. Because the eddy was not seen in this
simulation and the strong effects of tides and winds were turned off, it was concluded
that boundary nudging was not determining the existence of the Juan de Fuca eddy.

Simulation C used tides and upwelling winds but removed the influence of estuarine
flow from the eastern boundary. The initial conditions used were not those used in
previous simulations, but simpler — "identical initial temperature and salinity profiles,
typical of summer conditions off the Washington coast, were specified over the entire
model domain". The absence of this eastern boundary forcing removed the strong
northwest directed coastal current in simulation B. Despite this simulation establishing

an eddy off the coast of Cape Flattery, it is much weaker than simulation A, and does not share the same salinity patterns as simulation A. This suggests that the eastern boundary estuarine flow condition plays a significant role in the establishment of this eddy. It is not clear why the authors used different initial conditions here, and so these results may be suspect.

Simulation D removed tidal forcing from the model, but retained upwelling winds, and reintroduced estuarine conditions into the model. The eddy developed in this simulation was much stronger than the one in simulation A, suggesting that tides had an attenuating effect on the formation of the eddy. In this simulation, the eddy moved offshore and was centered over Tully Canyon. The authors make a point to say that despite this, Tully Canyon is not the origin of this eddy, but instead the eddy is generated as a result of strong upwelling off the coast of Cape Flattery, and then moves to Tully Canyon as it grows and detaches from the coast. Simulation E kept the forcing the same, but modified the initial conditions so that an eddy was not already present in the initialization. This was done to show that the eddy is formed as a result of forcing, not as a result of biased initial data. The eddy was shown to develop slowly, but the final output was said to be very similar to that of simulation A (in particular the salinity data and velocity fields were qualitatively identical).

Simulation F investigated the effect of the tides on the formation of the eddy. The wind forcing was turned off, but tides, estuarine flow and nudging conditions were used. It was shown that tides alone can cause enough upwelling to generate an eddy at the mouth of Juan de Fuca strait. The authors concluded that upwelling favourable winds were not a necessary component of the generation of this eddy, but played a role in intensifying the eddy.

Finally, simulation G modified the upwelling favourable winds to winter downwelling winds. A weak eddy was formed at the mouth of the strait, and so it was concluded that downwelling winds alone in the winter are not enough to suppress the formation of the Juan de Fuca eddy.

The results of these simulations show that the Juan de Fuca eddy can be generated

by: average summer upwelling favourable winds and an estuarine flow; tides and an estuarine flow; and all three mechanisms working together. It was also shown that upwelling favourable winds are not a necessity, and downwelling winds will still produce a cyclonic eddy at the mouth of the Strait of Juan de Fuca.

This study further investigates upwelling off the coast of Cape Flattery and the mechanisms that cause this upwelling. They will be summarized at a future time.

### 1.2.5 [Vindeirinho, 1998]; Currents, Water Properties and Zooplankton Distribution Over a Submarine Canyon Under Upwelling-Favorable Conditions

This summary is focusing on Chapter 2 of this thesis, title "Juan de Fuca Canyon". Despite the title, the study is largely focused on Spur Canyon. The primary study site is denoted as JF03 and is located near $48°15'N$, $125°12'W$, essentially on top of Spur Canyon. In addition to this on-canyon site, there was also a wind measurement site at Destruction Island, $47°41'N$, $124°29'W$.

The first set of analysis focuses on the correlation of wind direction at Destruction Island to current direction at Spur Canyon. It was found that even at 30m depth, the winds and currents were only weakly correlated, and this correlation decreased with depth. In an analysis of the salinity profiles, it was found that station JF03 at 30m depth was below the surface waters and was insulated from the wind, and so this decorrelation is not unexpected.

Looking at the current moorings at 30m, 75m and 200m, it is found that the prevailing currents in the top 75m are likely inducing the deep current at 200m. The 75m mooring shows that the current there is mainly cross-canyon and south to southeastward. It is found that the current weakens in August and turns northeastward (mostly eastward). At 200m in depth, the current is almost always northward, although it is stronger in July and August. This observation supports the expected summer upwelling events. The interpretation here is that the 200m current is up-canyon as a

response of the overlying 30m and 75m currents moving across-canyon.

## 1.2.6  [Thomson and Ware, 1996]; A current velocity index of ocean variability

Using the A1 mooring on the continental slope southwest of Vancouver Island, the currents were evaluated between October 1989-March 1995, and an index was created. The index is defined as:

$$I_v = \alpha \left| v_2' \frac{\partial v}{\partial z} \right| \frac{\partial v}{\partial z}, \qquad \alpha = -\text{sgn}(f) \left[ (f^2 + \delta^2)\sigma_v \right]^{-1}. \tag{1.1}$$

Where $\delta$ is a friction parameter, $\sigma_v$ is the standard deviation of the near-surface current velocity $v_s = \overline{v_s} + v_s'$, where $\overline{v_s}$ is the mean of the near-surface current velocity and $v_s'$ is the fluctuation about the mean.

It is noted that in section 2.3 of this manuscript, the authors prescribe a value of $\delta \approx 0.24 \times 10^{-5}s^{-1}$.

This index ($I_v$), based on velocity derivatives, has some definitive properties.

- "characterizes low-frequency baroclinic variability over the continental margin, and is linked, through the use of the thermal wind relation, to instability processes that effect the transfer of potential energy stored in the mean cross-slope density field to the kinetic energy of mesoscale meanders and eddies"

- along eastern boundary regions (i.e. BC coast region), the index ranges from large positive values during summer upwelling conditions to large negative values during winter downwelling conditions

- additionally, transition seasons (spring and fall) are characterized by $I_v \approx 0$

The authors go on to compare this velocity index to the Bakun index, which characterizes coastal upwelling conditions based on the wind-drive cross-shore Ekman transport.

## 1.3  Note on Spice as a Measurement

Spice is a commonly used quantity to describe the changing of water properties along an isopycnal surface. Water is "spicy" compared to a reference point if it is warmer and saltier. Water is "mintier" compared to a reference point if it is cooler and fresher. The mathematical definition for spice is shown in [Flament, 2002]. Simply speaking, it is a derived measurement chosen so that changes in spice ($\pi$) do not correlate to changes in $\sigma_\theta$. Full discussion of the state variable is available in [Flament, 2002].

## 1.4 Quick Summary of the Dynamics

**Water Composition in Area Around Spur Canyon**

Studied in [Mackas et al., 1987], the water around Spur and Juan de Fuca Canyons, near the shelf break is largely composed of CUC water below 50m depth (see figure 3 of [Mackas et al., 1987]). Meanwhile, the surface water is composed primarily of Offshore water far away from the coast, and outflow water from Juan de Fuca Strait nearer to the coast. Subarctic and Deep Undercurrent (denoted as Coastal Deep) waters are not important in these areas. It should be noted that the data used in [Mackas et al., 1987] is from August 1980, and so upwelling is expected.

**California Undercurrent properties**

The California Undercurrent is a northward flowing, deep current that is not seasonally effected. It moves along the west coast of the US and Vancouver Island. Following [Mackas et al., 1987], typical properties of the CUC are:

| | |
|---:|:---|
| Temperature: | 6.90 $°C$ |
| Salinity: | 33.90 psu |
| Nitrate: | 33.40 $\mu$mol |
| Phosphate: | 2.65 $\mu$mol |
| Silicate: | 52.00 $\mu$mol |
| Oxygen: | 2.10 mL L$^{-1}$ |

Table 1.3: Properties of the California Undercurrent, taken from Mackas, reformatted from previous table.

As stated in [Vindeirinho, 1998], the flow in the core of the CUC is generally northwest at 0.05-0.10m/s and is situated at a depth of 200-250m. Mooring data over Spur Canyon shows that the deep current is consistent throughout the year and it is the overlying current that changes seasonally. The seasonal change in this overlying current corresponds with the spring and fall transitions in the winds, however there is

typically a lag time (as demonstrated in [Freeland and Denman, 1982] , the winds and currents transition at different times, depending on the year; "the major seasonal cycles in currents are not strongly coupled to the local wind system").

[Hickey, 1979] documents the entire California Current System (CCS) in great detail (not summarized).

# Chapter 2

# Falkor Data

## 2.1 CTD Data from *CTD_GG* Directory

There are 6 primary stations here: JFG4a, LB08, BCC0, BCC1, LC12, MB07. They are summarized in figure 2.1.
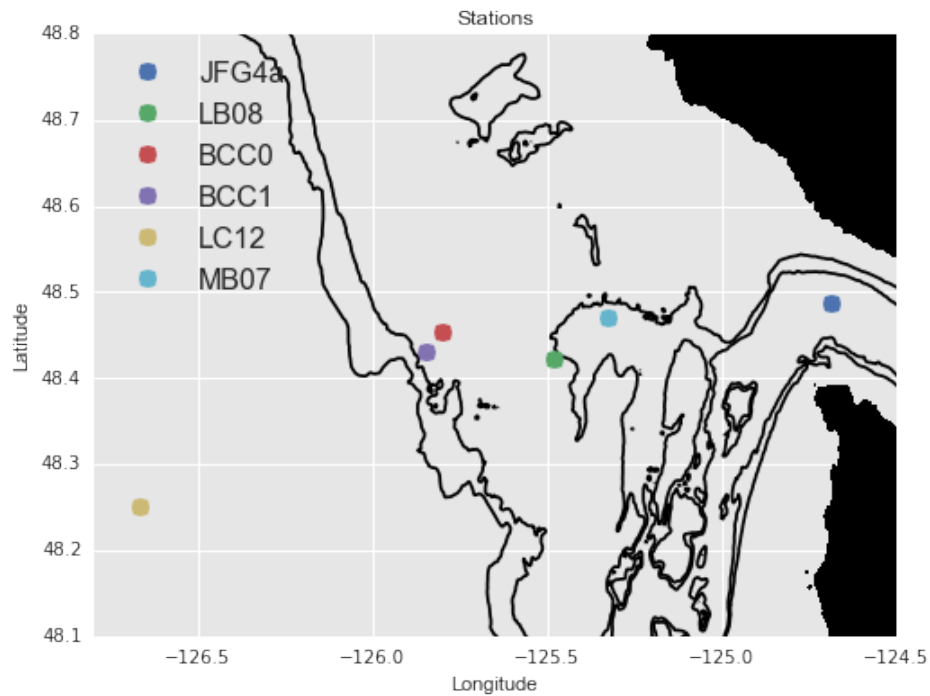


Figure 2.1: Locations of Falkor stations. Contour lines are the 150m and 200m isobaths.

### 2.1.1 Temperature-Salinity Data

TS diagrams were generated with corresponding 2D histogram data to see not only what the CTD data revealed about water composition, but also to see how much of each water mass was present in the data. Figure 2.2 shows this combined data. In addition to the raw CTD data (taken from directory *CTD_GG*), the data from [Mackas et al., 1987] of the five presented water mass tracer values for temperature and salinity are overlaid. [Mackas et al., 1987] report these values and use them to compare to CTD data from an August 1980 cruise.

It can be seen from this figure that California Undercurrent values from [Mackas et al., 1987] (represented by the purple-ish dot) appear to correspond with the clustered parts of the histogram data (red values on the color axis). Additionally, Juan de Fuca data (blue-ish dot) only appears in the JFG4a case. All cases show that the Offshore data (green dot) appears in the data, but not to a significant amount (in the sense that the green dot always appears along the TS line, but not in regions where there is a cluster of data points). Coastal Deep water (water beneath the California Undercurrent, roughly 400m in depth) only appears in the deepest station, LC12. Subarctic water is not seen in any samples.

### 2.1.2 Oxygen-Salinity Data

Similar plots are generated by using Oxygen data from [Mackas et al., 1987] and Oxygen data collected by the CTDs in the Falkor cruise. Figure 2.3 shows this. The oxygen values reported in [Mackas et al., 1987] are significantly higher than the values collected during the Falkor cruise (with the exception of Coastal Deep water). It is noted that the [Mackas et al., 1987] data was generated using historical data from 1959-1987, and so these values are certainly subject to change. However, it seems rather unlikely that these values would drop so dramatically, and so these results are to be taken with a grain of salt.
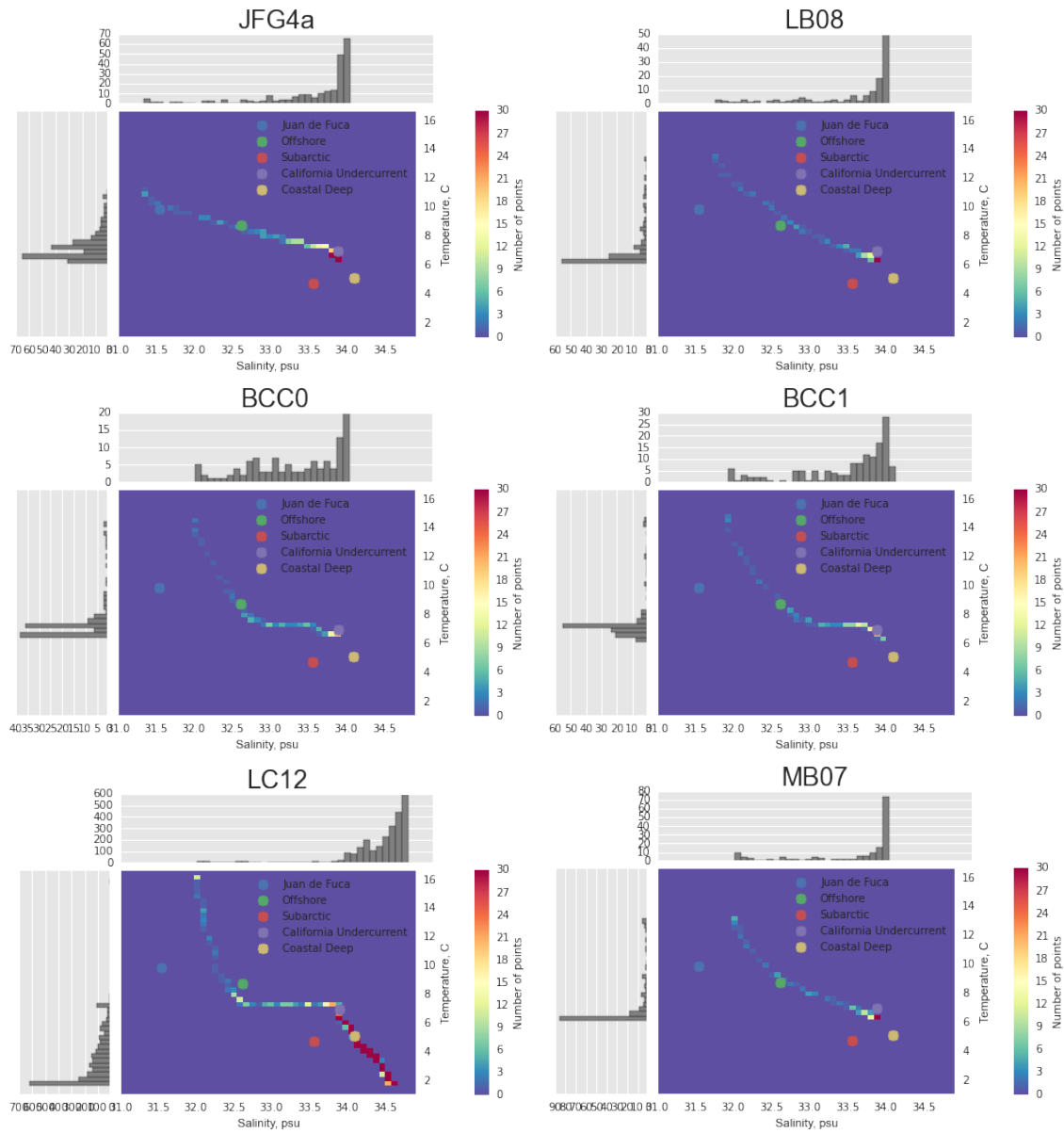
Figure 2.2: TS plots of Falkor stations. The overlaid circular markers denote the values given in Table 1 of [Mackas et al., 1987].
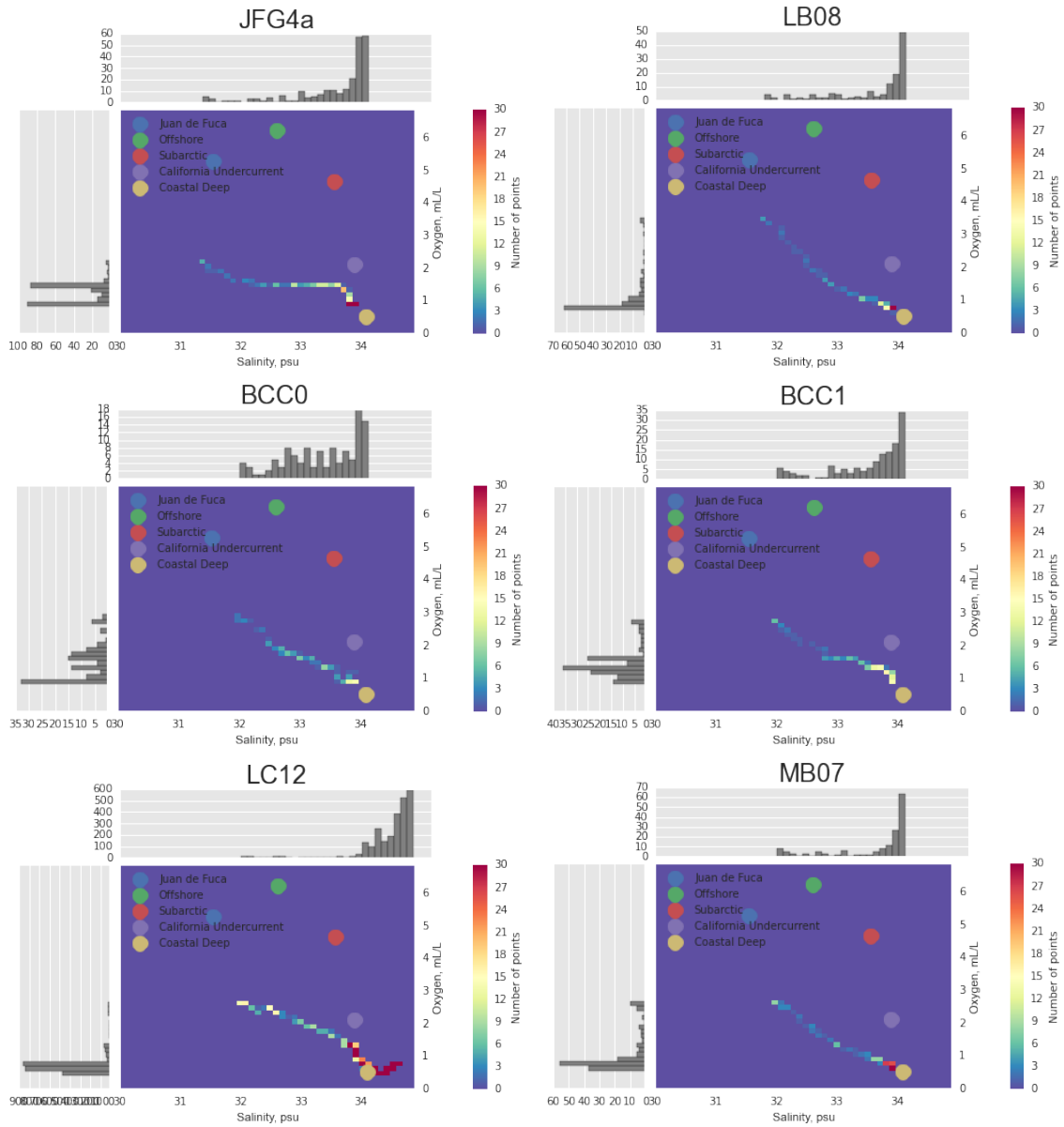
Figure 2.3: Oxygen-Salinity plots of Falkor stations. The overlaid circular markers denote the values given in Table 1 of [Mackas et al., 1987].

# Chapter 3

# NOAA data

## 3.1 Introduction

Data was downloaded from the NOAA World Ocean Database 2013. Using the WOD-select tool, requests for data in a lon/lat region between 160W-120W, and 15N to 60N were placed (much of the north Pacific ocean). CTD and OSD data were selected, giving both fine and coarse resolution temperature and salinity casts (although CTD data was used exclusively for these images). Data was downloaded in observed and standard levels.

Data may be found in CSV format in: `/ocean/rirwin/2_FALKOR_Data/5_WOD13_Data`. Several subdirectories are found here, created in chronological order – the most recent as of this writing is `WOD13_004`. All previously created subdirectories have data consisting of standard levels, whereas `WOD13_004` contains observed levels.

A python based parser for these files has been constructed:

`/ocean/rirwin/2_FALKOR_Data/2_Falkor_Upwelling_Repo/1_Notebooks/csvWOD.py`

This parser is rudimentary and only reads some pieces of the METADATA CSV section, and there is room for improvement. The resulting data structure is a python list of dictionaries. Each dictionary represents an individual cast; there are several keys that hold different values/variables etc. Documentation for this code should be

put together.

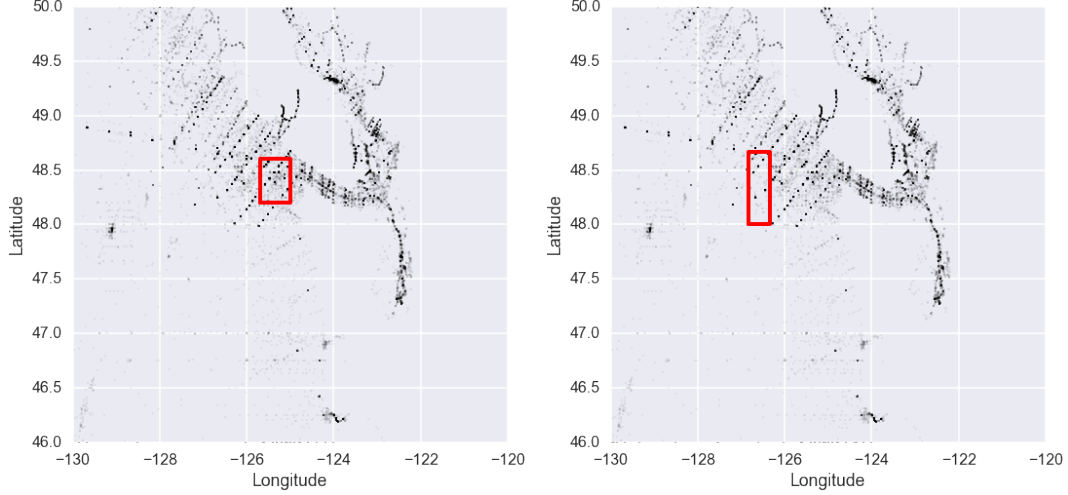## 3.2 Investigating NOAA Data using Observed Levels



Figure 3.1: Left: Region around MB07, Right: Region around LC12. Each black dot represents an individual cast from NOAA data.

### 3.2.1 MB07

The MB07 coordinates are $(125.325W, 48.470N)$. A region is defined around this point between $125°W - 125.7°W$, and $48.2°N - 48.6°N$. All casts not in this region are filtered out of the NOAA dataset, and the remaining casts are analyzed. The following figure, (cite TS fig), shows the monthly temperature-salinity plots for this specified region.

There is a sparsity of casts in January, November, and December, but all other months seem to have a significant number of casts. The blue line is representative T-S line for each month. The overlaid red dot in each casts represents the Falkor '13 eddy water values, $6.3°C$ and $33.9psu$. It can be seen that the eddy water value is only

Figure 3.2: Temperature-Salinity data in the MB07 region, divided into months. The red dot represents the Falkor '13 eddy water data.

near the rest of the data from May-Sept, and doesn't appear in the dataset for other months.

The trend in data is not surprising for a coastal system. In the summer months, the surface waters are warmed and a slope is introduced into the T-S diagram. In September, the surface waters begin cooling and introduce a bend in the curve. Once these surface waters are cooled, the slope flattens out. The deeper waters tend to cool in the summer months and warm in the winter months (although there is a lack of data).

### 3.2.2   LC12

Looking at the TS plots for LC12, figure 3.3, it is apparent that this region is distinct from MB07. Despite the two regions being separated by roughly one degree of longitude, the TS curves are very different. In particular, there are three distinct parts of the LC12 curve for the summer months (June-Oct).

- Temperature stratified surface waters – characterized by high surface temperatures, rapidly dropping to lower temperatures, with salinity changing between 31-32.5psu.

- Salinity stratified intermediate waters – temperature remains consistent between 7-9°$C$, however the salinity changes from 32.5-34psu.

- Temperature stratified deep waters – temperature rapidly decreases between 7-2°$C$, while salinity is between 34-35 psu.

It is also apparent that the Falkor '13 eddy water may be represented by at least some parts of the water column for each month of the year (the red dot appears to intersect the black dot region for each month). It appears to happen around the transition from intermediate to deep waters – right around the second knee of the TS curve.

### 3.2.3   What Defines Eddy Water?

Water characteristics vary with time – month-to-month, year-to-year, etc. How does the JdF eddy water change with time?

**Annual Variation, Aug-Sept**

The Falkor Cruise data was collected near the end of August, 2013. Let's compare NOAA data from Aug-Sept of each year where sufficient data is available. We define eddy water as the point of a 2D T-S histogram that contains the highest amount of cast

T-S vs Month for Area Around LC12
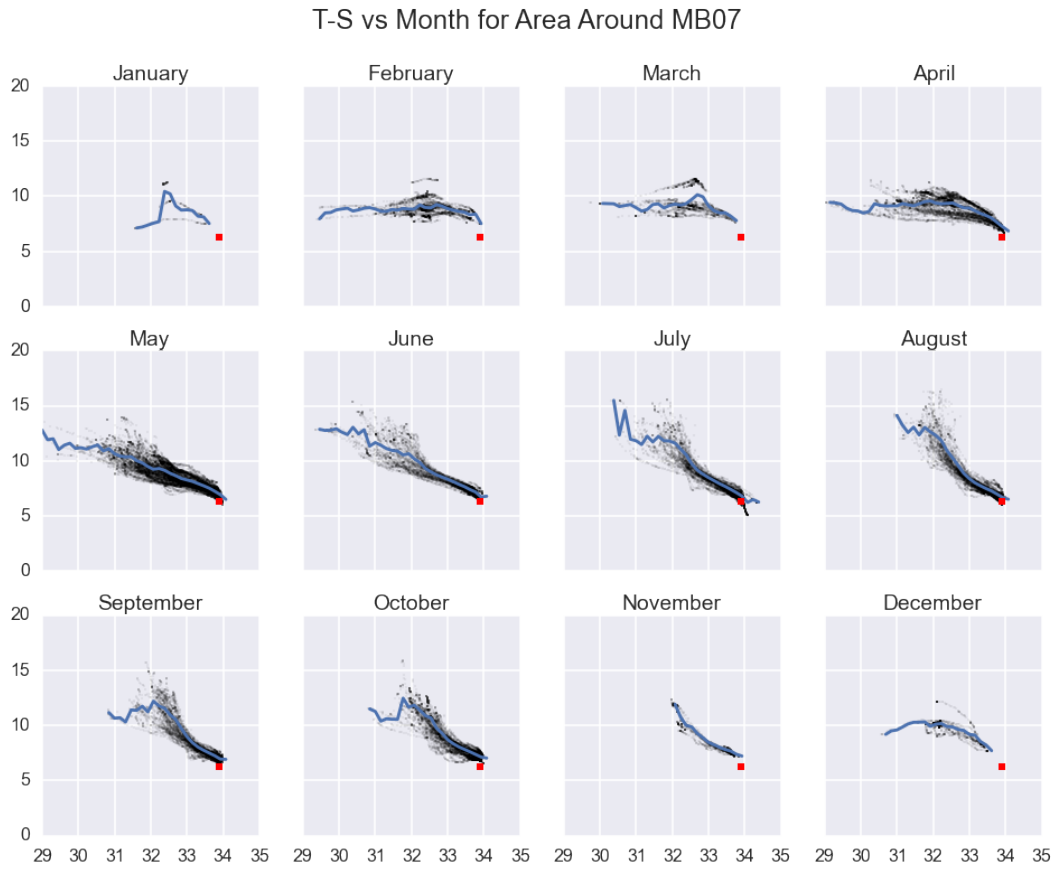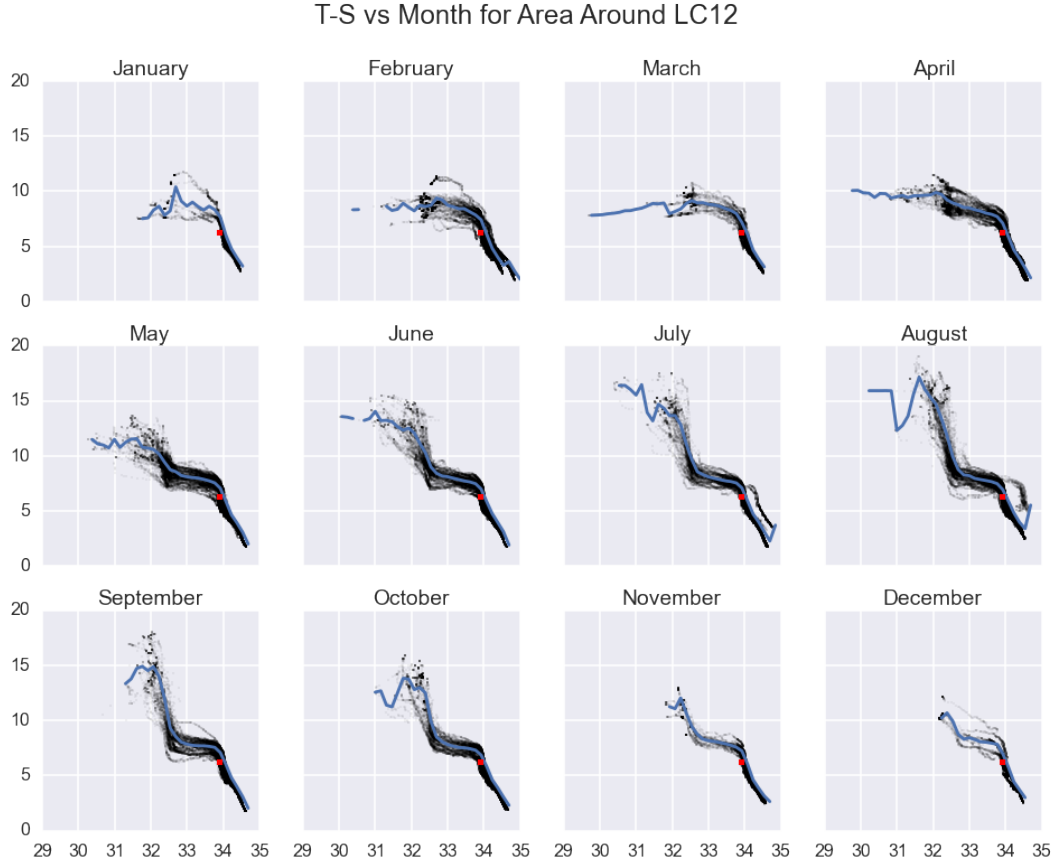


Figure 3.3: Temperature-Salinity data in the LC12 region, divided into months. The red dot represents the Falkor '13 eddy water data.

data (similarly to how eddy water was defined for the Falkor data). Effectively, it may be said to be the binned T-S mode of the system. Figure 3.4 shows the interannual variability of binned T-S mode data for salinity, temperature and potential density anomaly.

Beginning with salinity, the minimum T-S mode salinity was roughly 33.75psu, while the maximum was calculated to be roughly 33.9psu (around the Falkor data). Perhaps not physically important, there appears to be a $\sim 6$ year cycle in salinity, with salinity steadily increasing over 6 year spans, then decreasing dramatically the following year. The mean eddy water salinity is roughly 33.85psu.

Temperature has less structure than the interannual salinity variability field. The mean value of eddy water temperature is $6.8°C$, although the range is from $6.3$-$7.2°C$.

The Falkor data is at the low extreme of data.

Finally, the potential density anomaly is approximated (the long term mean depth was used to calculate this data, and so it must be refined to get a more exact value). The mean $\sigma_\theta$ value hovers around $27.3kg/m^3$, with variation $\pm 0.1kg/m^3$.
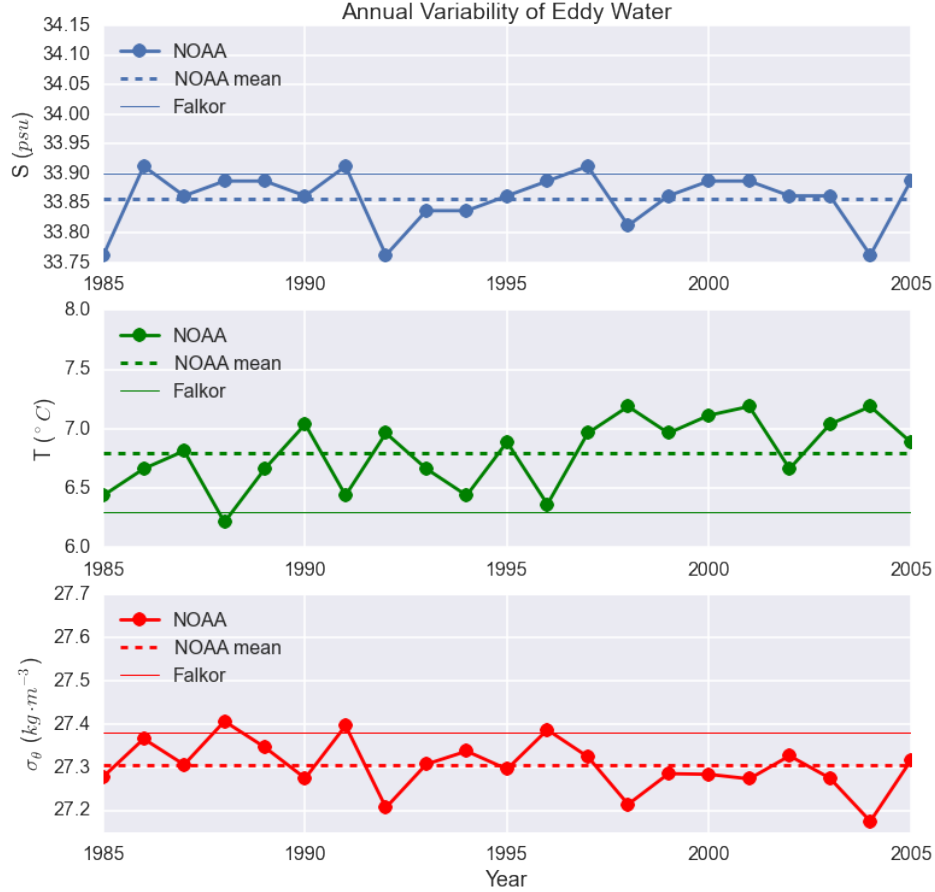


Figure 3.4: The annual variability of August-September water in the eddy region.

## 3.3  Investigating the JdFE Region

*Note: the abbreviation 'ER' will be changed to 'JdFE Region' as a more descriptive term.*

Here, we focus in specifically on the eddy region and discuss the ways in which the

water is defined. One limitation of the previous analysis was that the "eddy water" definition was fixed based on 2013 data (two casts of 2013 data specifically). Of course this water mass changes annually and interannually, and we must create a definition of what eddy water actually is. To do this, we must define the eddy region.

For the purposes of this study, the eddy region is based off of two papers, [Freeland and Denman, 1982, Thomson and Ware, 1996]. The region is approximated based on figures showing the upwelling centre (figure 5 [Freeland and Denman, 1982]), and a sketch of the prevailing summer current patterns (figure 3 [Thomson and Ware, 1996]). Using these two figures as guidelines to define the region, a rectangle is defined between latitudes $48.2°N - 48.6°N$ and longitudes $124.8°W - 125.6°W$.

### 3.3.1 Annual Maps

In this section, look at annual surface maps at various depths for various fields (salinity, temperature, etc.).

The maps are calculated by taking all available casts for each month and interpolating the results from a point-by-point cast value at specific depth (interpolated linearly if necessary), to a regular grid (50x50 in this case). The data is interpolated to the regular grid by using the nearest neighbour value for each point. These approximations may lead to some errors (but no quantifications for these errors are presented). Nonetheless, the annual trend appears to be evident here.

Looking at the $50m$ depth image, it shows that beginning in May, some high-salinity water is upwelled along the northern part of WCVI. As the upwelling season progresses, this high-salinity water appears in souther parts, in particular around JdF and Spur canyons. It isn't until December when the traces of this high-salinity water disappear.

### 3.3.2 Defining the T-S Mode

The T-S mode is what is essentially eddy water in the JdFE region (named as such because it is the T-S bin with the highest frequency of occurence, hence "mode").
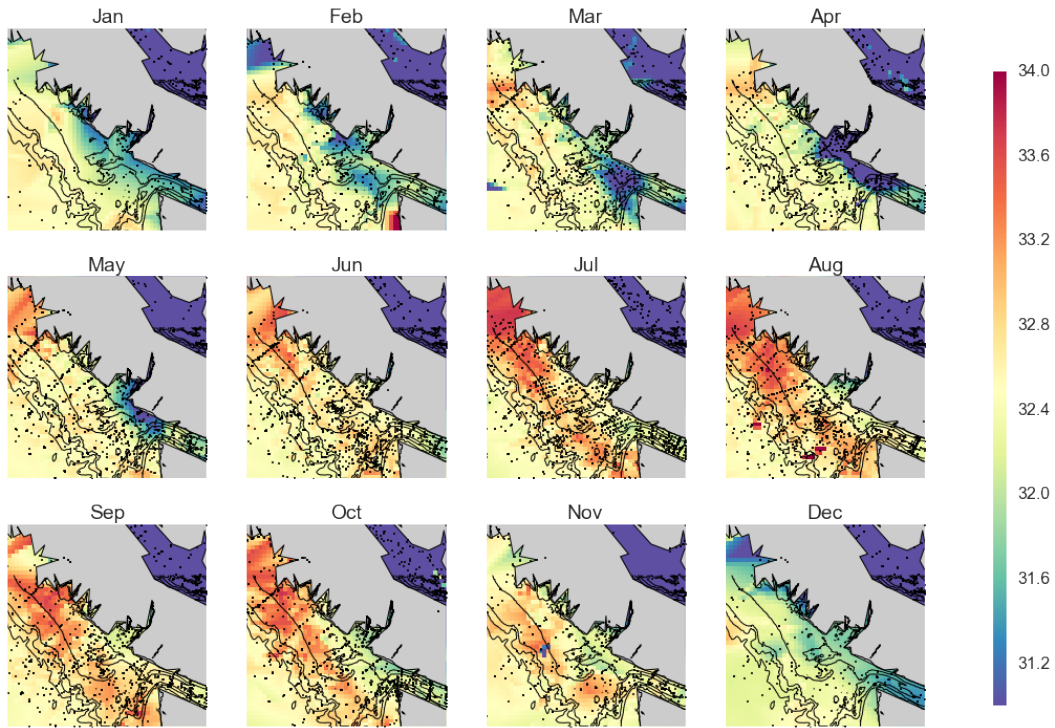
Figure 3.5: Looking at the salinity around the JdFE region at 50m depth.

## 3.4   Plots Generated Using `JdFE_v02.dat`

### 3.4.1   Monthly Density Profiles

Figure 3.9 shows the monthly density profiles using the aggregated data. Note that December and January have very few casts available in the JdFE region, and so the analysis applied to these months will be relatively inaccurate/insignificant.

A basic trend is apparent in the surface waters – in the winter months, the surface waters mix and become more uniform. As the year progresses, the surface waters warm and become stratified, leading to a more pronounced profile. The deep water changes are less apparent from this image.
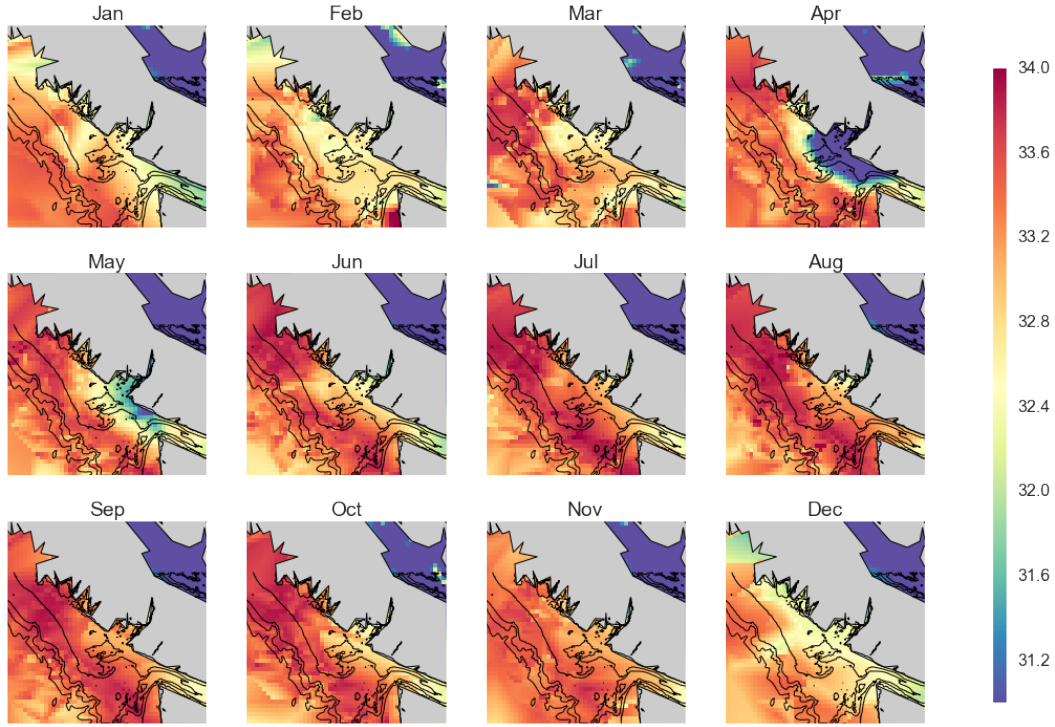
Figure 3.6: Looking at the salinity around the JdFE region at 100m depth.

## 3.4.2 Depth of the $\sigma_\theta = 26.5 kg \cdot m^{-3}$ Isopycnal

The depth of the California Undercurrent core density surface is plotted across the domain as a function of month (figure 3.10). In the red outlined box, it is evident that the depth of this surface shallows beginning in March, and becoming evident in June. It becomes very shallow in August and September before rapidly disappearing in November. If nothing else, this image serves to show where the eddy spins up and approximately when it spins up. It is not clear whether the surface shallows south of the eddy region as a result of the eddy spinning up, or whether the eddy spins up as a result of the south surface shallowing.

## 3.4.3 Coastal Cross-Section (June-August)

Vertical profiles are patched together along a transect along the California Undercurrent pathway for casts taken between June and August.
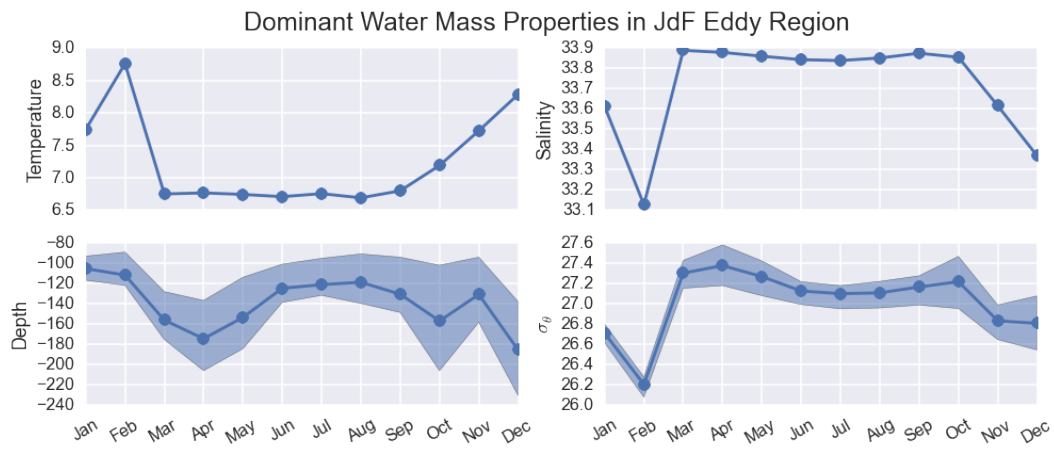
Figure 3.7: The average annual variability of the T-S mode. Temperature, salinity, depth range (20-80 percent quintiles), density range (20-80 percent quintiles). Note the sharp transition in March, persistent until September, and transitioning until February.
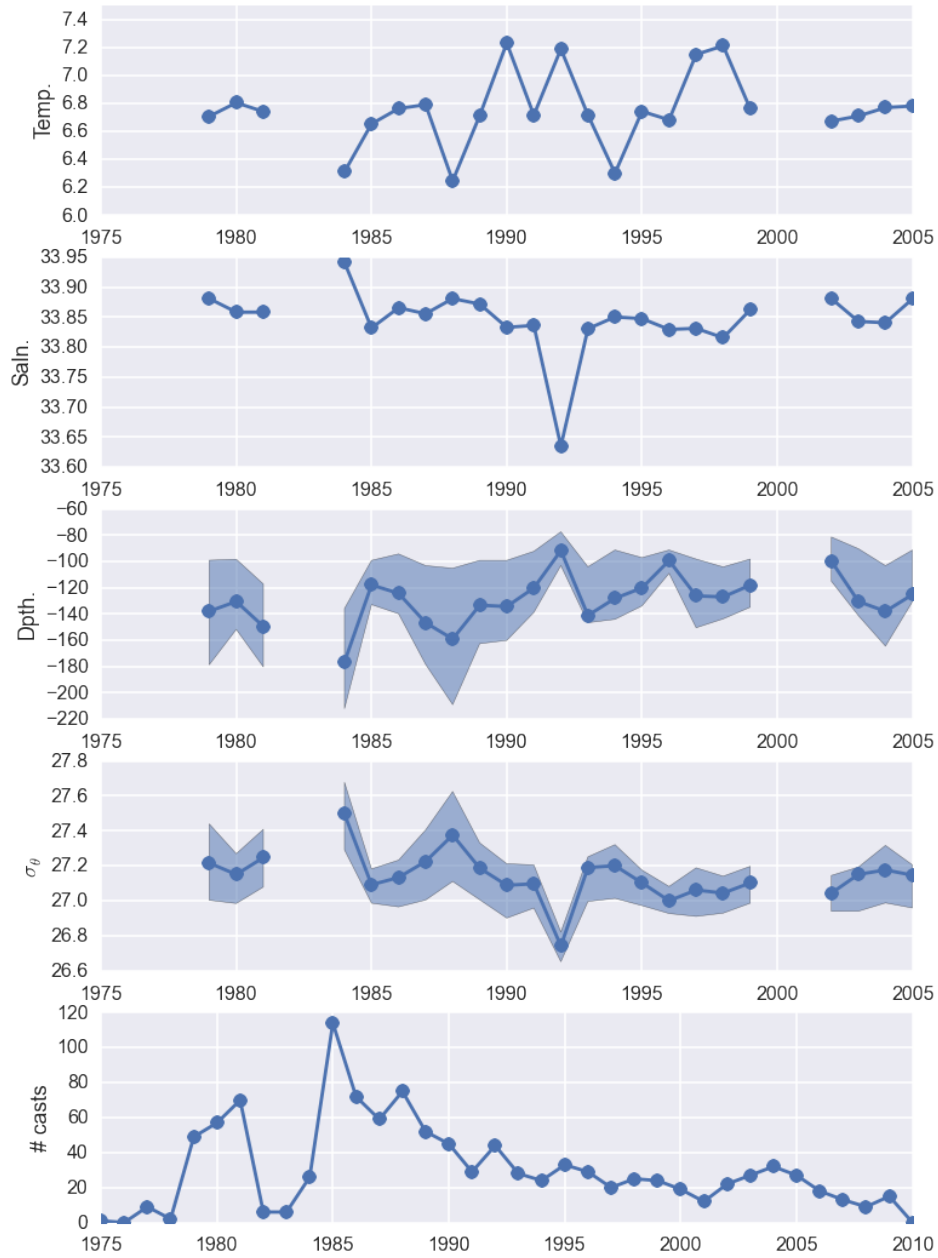
Figure 3.8: The average interannual variability of the T-S mode. Beginning with the top plot: temperature, salinity, depth of mode (20-80 percent quintiles), range of density surface (20-80 percent quintiles), and annual number of casts. All data shown for years with minimum 20 casts (except last plot).
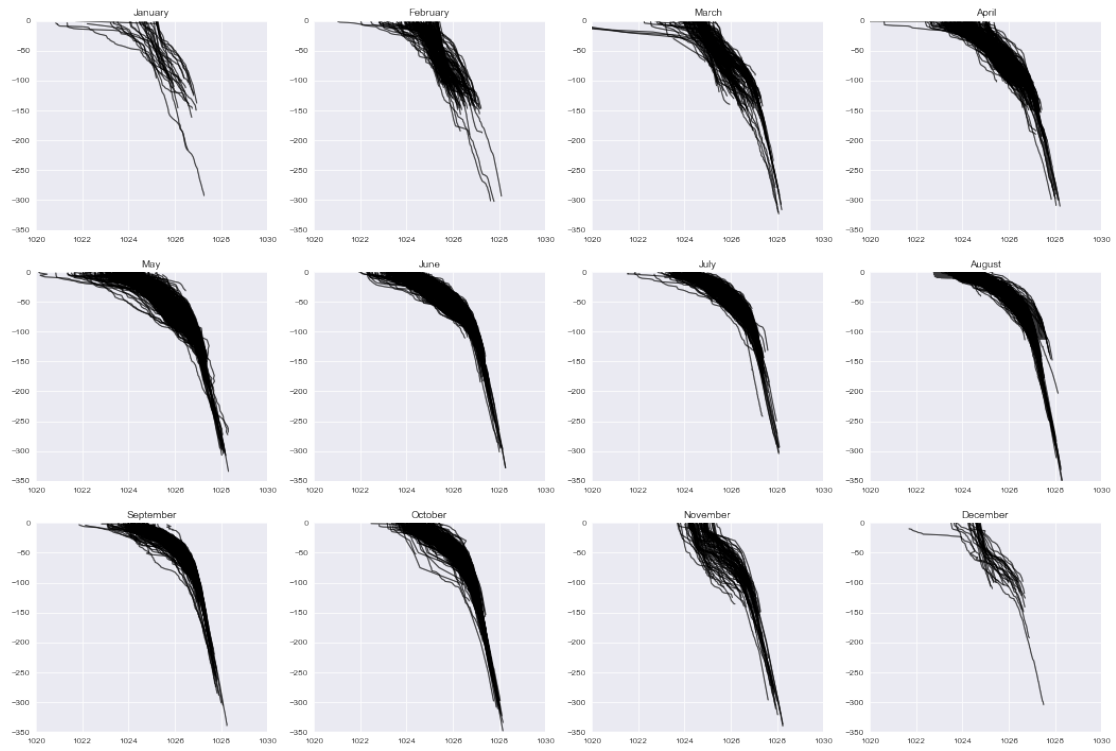
Figure 3.9: Monthly density profiles using the JdFE v02 data file (includes IOS data).
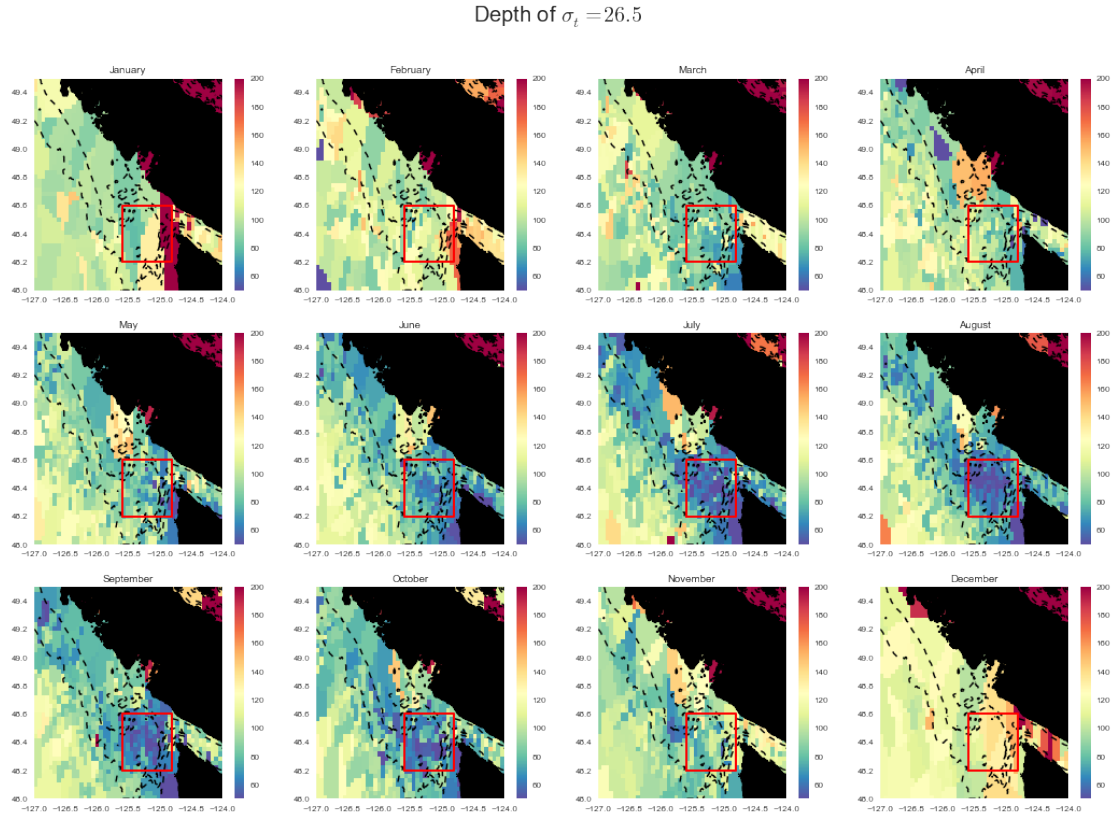
Figure 3.10: The depth of the $\sigma_\theta = 26.5$ surface as a function of month. Outlined in the red box is the JdFE region.
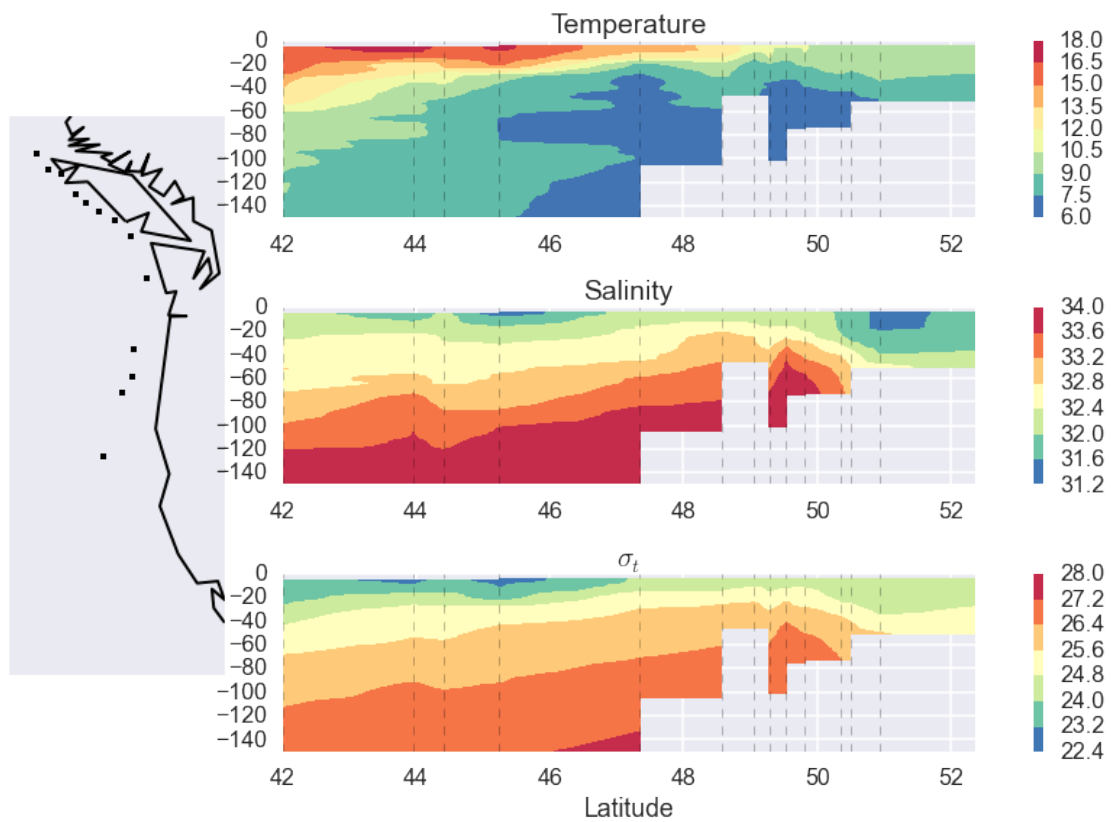
Figure 3.11: A cross section of temperature, salinity, and density surfaces along the coastal transect.

# Chapter 4

# Users Guide

## 4.1 Directory Structure `/ocean/rirwin/2_FALKOR_Data`

In this directory, there are several subdirectories.

### 4.1.1 `0_Cruise_Report`

The FALKOR cruise report, put together by members of the 2013 cruise. Summarizes findings – shows CTD casts, tracks, etc. Report found in `0_Final_Report.pdf` within directory.

### 4.1.2 `1_Papers`

Collection of most of the papers summarized in this report.

### 4.1.3 `2_Falkor_Upwelling_Repo`

Contains most of the analysis and this `.tex` file. Subdirectories: `0_TeX` and `1_Notebooks`.

### 4.1.4   3_Repo

The FALKOR cruise bitbucket repository. Contains some ipython notebooks of the initial analysis.

### 4.1.5   4_Notes_Susan

Contains a `.pdf` with two pages of Susan's notes on the eddy water around MB07 and LB08.

### 4.1.6   5_WOD13_Data

Contains four subdirectories at the time of this writing. Sorted in chronological order, with `004` being the most recent iteration of `.csv` files taken from the WoD online.

### 4.1.7   6_IOS_Data

Contains the raw data from Roy Hourston at IOS. I believe there are six different file types: `.bot, .ctd, .che, .BOT, .CTD, .CHE`. These files can be read in with `ios_read.py`.

### 4.1.8   7_Falkor_CTD

Contains the CTD files from the FALKOR cruise. Somewhat deprecated, as this information is also found in the IOS data.

## 4.2   CTD readers

There are three components to the CTD readers: NOAA WoD reader, IOS reader, and an aggregated reader. Users should only have to deal with the aggregated CTD reader (shortened to 'ACTDR').

### 4.2.1 Aggregated CTD reader

The purpose of this module is to take both IOS and NOAA data from the separate databases and combine them into one large Python list of standardized dictionaries. This will allow for seamless viewing/processing of CTD data. In addition, this module allows for Python pickling/unpickling of the database, which should reduce readtimes significantly. Finally, the database also provides a simple procedure for removing duplicate cast information so that data is not overrepresented in the final database.

**Loading a database**

For a database compiled using ACTDR, loading it into a Python script is straightforward:

```
1  # load in the module
2  import ACTDR
3  # load the database into the module
4  ACTDR.load_dat('DBfile.dat')
```

This loads the database file into the global variable `ACTDR.CTD_DAT`.

**Compiling a database**

If new data becomes available, or if the standard keys are changed, then the database must be compiled again. The way that the code is currently setup is to look for .CSV WoD files in one directory, and IOS files in another directory.

The first step is to add files into the appropriate directory. For CSV WoD files, this directory is:

`/ocean/rirwin/2_FALKOR_Data/5_WOD13_Data/WOD13_004/`

For IOS data files (.ctd, .CTD, .bot, .BOT, .che, .CHE), this directory is:

`/ocean/rirwin/2_FALKOR_Data/6_IOS_Data/`

Note: the .bot/.che/.BOT/.CHE files seem to be too low quality/too low resolution for this analysis and probably should not be included when reading the IOS database.

After adding these files to the appropriate directory, run the following script:

```python
# load in the module
import ACTDR

ACTDR.load_noaa() # load WoD data
ACTDR.load_ios() # load IOS data
ACTDR.remove_duplicates() # remove duplicate casts
ACTDR.filter_year(1970) # removes any casts from before 1970
ACTDR.filter_keys () # filters data with 'None' keys or bad values
ACTDR.filter_anom() # filter anomalous casts -- i.e. casts with -100 psu
    salinity, etc.
ACTDR.save_dat('filename.dat') # save to file
```

This is a very long process. Currently, with 100000+ casts from NOAA and 10000 from IOS, this script takes more than an hour to complete on Snapper. About half of the time is spent in the `remove_duplicates` function, so there is some time savings to be had by optimizing that function.

**Working with the database**

Here's a simple example showing the T-S diagram of every single cast available in the database `DB_v01.dat`.

```python
import matplotlib.pyplot as plt
import ACTDR

ACTDR.load_dat('DB_v01.dat')

plt.figure(figsize=(8,8))

# the following two lines are double list comprehensions
S = [x for k in ACTDR.CTD_DAT for x in k['Salinity']]
T = [x for k in ACTDR.CTD_DAT for x in k['Temperature']]
plt.plot(S,T,'.k')
plt.show()
```

**Current Database**

The most current database is an aggregation of the NOAA and IOS data, with duplicates removed and filters. The database was generated from raw data using the following script:

```python
import ACTDR # import the module

ACTDR.load_noaa() # load the NOAA data
ACTDR.load_ios() # load the IOS data
ACTDR.remove_duplicates() # remove any duplicates
ACTDR.filter_year(1970) # remove any data before 1970
ACTDR.filter_keys() # remove any 'None' data
ACTDR.filter_anom() # remove any anomalous data

ACTDR.save_dat('DB_v01.dat') # save the DB
```

This database has 114582 casts from 1970-2014 (filtered from 185717 casts). The distribution with respect to year is summarized in figure 4.1
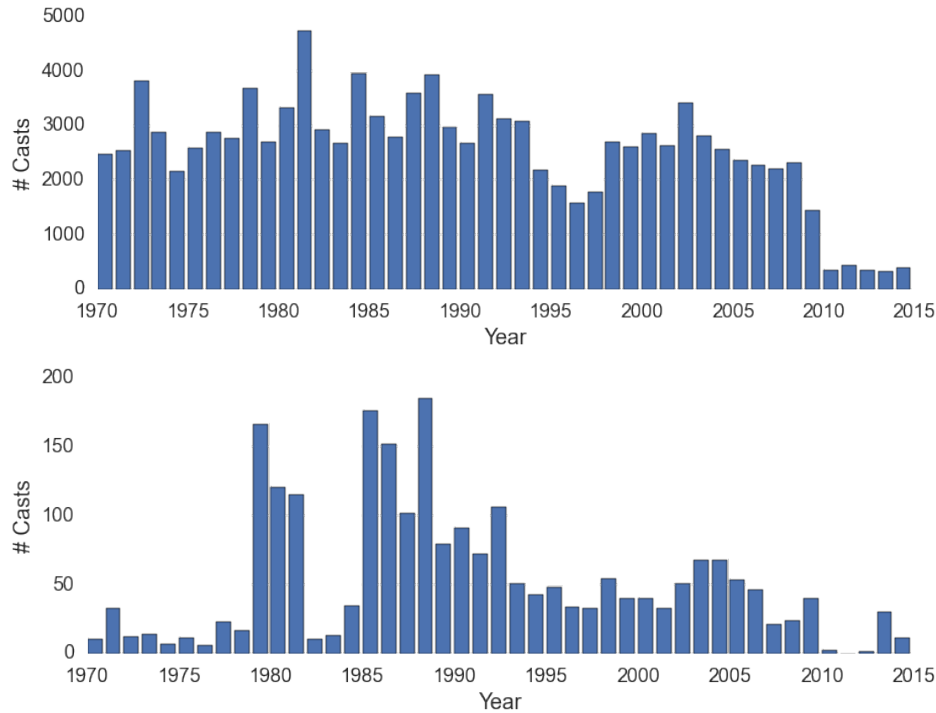


Figure 4.1: *Top:* The distribution of casts in the DB_v01 database. *Bottom:* The distribution of casts in the JdFE_v01 database.

In addition to the `DB_v01` database, a database was created including only casts within the JdFE region defined before. This database is named `JdFE_v01`. The annual distribution of casts is highlighted in figure 4.1. There are 2347 casts in the `JdFE_v01` database.

The `JdFE_v01` database is generated from the following code (assuming that `DB_v01` is already loaded into the Python environment).

```python
import ACTDR # import module
ACTDR.load('DB_v01.dat') # load in the full DB

rm_ind = [] # rm_ind contains the indices to remove

# loop through all casts
for ii,cast in enumerate(ACTDR.CTD_DAT):
    # see if cast is outside of eddy region
    if cast['Latitude'] < 48.2 or cast['Latitude'] > 48.6 or
        cast['Longitude'] < -125.6 or cast['Longitude'] > -124.8:
        rm_ind.append(ii) # append to the remove list if outside

# loop through the removed indices list
for ii in rm_ind[::-1]:
    del ACTDR.CTD_DAT[ii] # delete said index

# let the user know the new number of available casts
print '> ', len(ACTDR.CTD_DAT), ' casts'

# save the new DB
ACTDR.save_dat('JdFE_v01.dat')
```

**Adding variables to database**

Currently, the standardized format only has salinity, temperature and depth being saved as arrayed variables for each cast. If oxygen, or other nutrients become necessary to save, this would require a rewrite of how the standardizing function works. There are two primary functions that must be changed here: `convert_ios_dict` and `convert_noaa_dict`, and also the global variable `STANDARD_KEYS` must be updated.

The following is an example of how to add oxygen measurements to the database.

Step 1, change the `STANDARD_KEYS` variable at the top of ACTDR.py to include `'Oxygen'`:

```
STANDARD_KEYS =
    ['Longitude','Latitude','ID','Day','Month','Year','Temperature','Salinity','Depth',
     'Oxygen']
```

This forces the `convert_..._dict` functions to create an `Oxygen` key for each cast.

At this point you will have to see how the NOAA and IOS data files save oxygen information in their files. This is what determines their key in the NOAA and IOS dictionary variables. Then you will have to include if/then statements in the `convert...` functions to test whether oxygen is included on a cast-by-cast basis.

### 4.2.2 Versions

**v01**

Initial version. Standard keys include:

```
STANDARD_KEYS =
    ['Longitude','Latitude','ID','Day','Month','Year','Temperature','Salinity','Depth']
```

**v02**

Added $\sigma_t$ information in new key: `sigmaT`. Density calculated using `seawater` module. Any `np.nan` values were interpolated over for the `sigmaT` field. Only two databases in v02: `DB_v02.dat` and `JdFE_v02.dat`.

# Chapter 5

# Eddy Generation Hypothesis

There are several factors/physical systems that overlap in the area of the JdFE. Among these, the primary physical systems/phenomena will be identified (in no particular order:

- Estuarine circulation in Strait of Juan de Fuca

  The outflow regime is primarily in the surface $60m$ [Thomson et al., 2007], while the inflow regime is below this depth. This estuarine flow is most dominant in summer, and less dominant in winter. It is shown in [Foreman et al., 2008] that this circulation is largely responsible for the initial generation of the eddy.

- Vancouver Island Coastal Current (VICC)

  This feature may add to the surface cyclonic vorticity of the eddy as water is transported poleward.

- Vancouver Island Shelfbreak Current (VISBC)

  This current appears centered over the $200 - 250m$ isobath off the coast of Vancouver Island. As the upwelling season begins, it is hypothesized that this current moves landward, towards the VICC. The currents are shielded from each other in the area around the La Perouse Bank due to the topographic gradient, however south of this bank, it is flatter, and so it is hypothesized that the two currents may

induce a shear instability, contributing to the initial surface JdFE generation.

- California Current System, specifically California Undercurrent (CUC)
  This large, slow moving current is shown by [Mackas et al., 1987] to contribute significantly to the JdFE. However, knowing that this current is deep and is poleward moving, it must traverse the steep rim of the JdF canyon to contribute to the eddy dynamics. This water is hypothesized to be upwelled from March-August through Spur Canyon (so as to be consistent with [?] findingsand the suggestion of [Foreman et al., 2008]).

- Tides
  Not thought to be important until reading [Flather, 1988], the $K1$ tidal component appears to form an-eddy like pattern near the JdFE (figures 3/6 of [Flather, 1988]). Additionally, [Foreman et al., 2008] shows that tides play a significant role in sustaining the eddy and inducing the initial upwelling off the coast of Cape Flattery.

## 5.1   Annual Isopycnal Cycle

March to August represents the time when the eddy is present, and upwelling is evident here. The $27.2 kg \cdot m^{-3}$ surface shallows from $150m$ to $125m$, salinity remains relatively consistent ($33.9psu$), while temperature drops somewhat from $7°C$ to $6.7°C$. This trend of consistent salinity, decreasing temperature, and shallowing depth is consistent for deep isopycnals ($\sigma_t > 26.5 kg \cdot m^{-3}$). For shallow isopycnals (green and blue curves), the shallowing is consistent, however there is a definitive trend of increasing salinity and temperature (highly amplified near the surface).

This increasing temperature and salinity is consistent with the Foreman hypothesis that deep coastal water is upwelled through JdF canyon, and brought up in the surface $60m$ near Cape Flattery, where it mixes with the estuarine outflow from the strait, and is transported westward to the JdFE.

## 5.2 Visualizing the Generation of the Juan de Fuca Eddy

To visualize this process, the $26.0kg \cdot m^{-3}$ isopycnal is used. NOAA data and IOS data are interpolated onto a regular grid to show the approximate mean depth of this isopycnal for a given month. In March, it can be clearly seen that along the Washington coast, and near Cape Flattery, the surface is shallowed to roughly $50m$. Moving from March to May, this shallowing intensifies along the coast to $30m$ and is beginning to travel west. By June and July, this isopycnal is showing a clear dome shape centered on the JdFE. Upwelling is still very evident along the Washington coast.

However, looking at just the $27.2kg \cdot m^{-3}$ surface, and seeing how it changes annually, (figure 5.3), it is evident that the TS mode "eddy water" is not transported from Cape Flattery. Instead, it appears that the eddy water is largely transported from the northwest of the JdFE region and from the south (possibly up Spur Canyon). This is evidenced in figure 5.3, as bands of similar depth surfaces are seen to the northwest and south of the region between March and September.

A feature of an upwelling eddy is doming isopycnals. This is difficult to visualize with interpolated data, due to the fact that it is messy and "spiked". Instead, the interpolated data will be heavily filtered to look exclusively at large scale features. Looking at figure 5.4, a sense of where the eddy forms along the $48.5°N$ parallel can be had.

The filter used is an even Fourier filter (with only the first 4 wavenumbers kept). As a simple description, the field that is being filtered is extended in an even way, and a Fourier transform is taken. Because the field is extended in an even way, only the cosine (real) part of the Fourier coefficients are present. The short wavelength (large wavenumber) parts represent small scale features of the field, and are not of interest, and so they are set to zero. An inverse transform is performed on the filtered field. After the inverse transform is performed, only the first half of the array is kept (because

the transform was done under the extended field). This yields an aggressively filtered field.

## 5.3   Outstanding Questions

### 5.3.1   The Deep Water Upwelling Mechanism

The eddy generation process for the surface $\sim 80m$ of the eddy water column has been shown to originate off the coast of Cape Flattery, and then advect westward as a result of Juan de Fuca Strait outflow. The eddy itself however, shows that upwelling occurs throughout the water column, not just the surface $\sim 80m$. This leads to the first outstanding question:

   1) What is the mechanism through which deeper water is upwelled in the JdFE region?

See figure 5.4. The deep isopycnals are seen to deflect upwards, showing a "dome" shape consistent with a cyclonic eddy. This doming of isopycnals in late summer (August/September) is complete through the water column, suggesting that the eddy is barotropic by this time of year. However in the early part of the upwelling cycle (April/May), the surface isopycnals are shown to have some dome-like feature, however the deep isoycnal does not. This may suggest that a different mechanism generates the deep cyclonic vorticity necessary to sustain upwelling at depth.

This may be seen in more depth in figure 5.3. In March, the isopycnal is deflected upwards near the shelf-break. This is consistent with coastal upwelling – an adjustment to the spring transition. This shallowing along the shelf-break is seen until August/September. It should be noted that the shallower $26.0 kg \cdot m^{-3}$ isopycnal did not show this behaviour, suggesting that this coastal upwelling is limited to deep water. As a preliminary hypothesis for the deep eddy water origin:

   Eddy water originates from the deeper ocean waters and is upwelled onto continental shelf through standard coastal upwelling. It is then advected southward as a result of

the shelfbreak current that is prevalent in the spring/summer months, and is deflected eastward toward the eddy as a result of the complex topography in the region – a very rough hypothesis would suggest that the La Perouse bank may be responsible for deflecting this water eastward towards the eddy region, but this is only speculation.

## 5.3.2    The Role of Spice

One area of primary interest that will certainly be a direction for future study is:

> 1) How can we use the measurement of spice to tell us about the origins/-pathways of eddy water?

Spice may be used as a tracer to identify how water moves from one location to another, and this problem here is perfect for this approach. In particular, calculating spice along isopycnals will give a rough idea of what the individual water masses are and how important each source of water is for eddy generation. There are several potential sources of water:

- Juan de Fuca Strait outflow water

- California Undercurrent water

- Vancouver Island Coastal Current water

- Shelfbreak water

- Coastal deep water (upwelled from below the shelfbreak)

- Juan de Fuca canyon water (is it different from coastal deep water?)

Other sources may include Alberni Inlet outflow/any small river outflow from WCVI, and California Surface Current waters.

### 5.3.3 Visualizing Geostrophic Flow

The gradient of isopycnals can be determined from NOAA/IOS data and so the geostrophic currents in the region can be approximated by looking at smoothed/filtered maps of isopycnal deflection. This overall geostrophic flow could be used to map out dominant currents at various depths, and could give a very clear picture of exactly where water is coming from as it enters the JdFE region. Data must be filtered, as it is fairly spiked (due to so much data from so many instruments and so many years being aggregated), and I suspect that an aggressive filter would have to be used to get isopycnal slopes/gradients at geostrophic scales.

Another limitation of this would be getting an appropriate topographic map of the area. I am not sure if anything that I currently have would be sufficient.

> 3) What do the geostrophic flows look like in the area? Is the deep water generated as a result of large-scale upwelling along the coast, and can we trace it's origin through maps of geostrophic flow?

If the deep water was being upwelled through Spur Canyon as a result of pressure gradient/Coriolis imbalance, then this would not be seen in geostrophic currents.
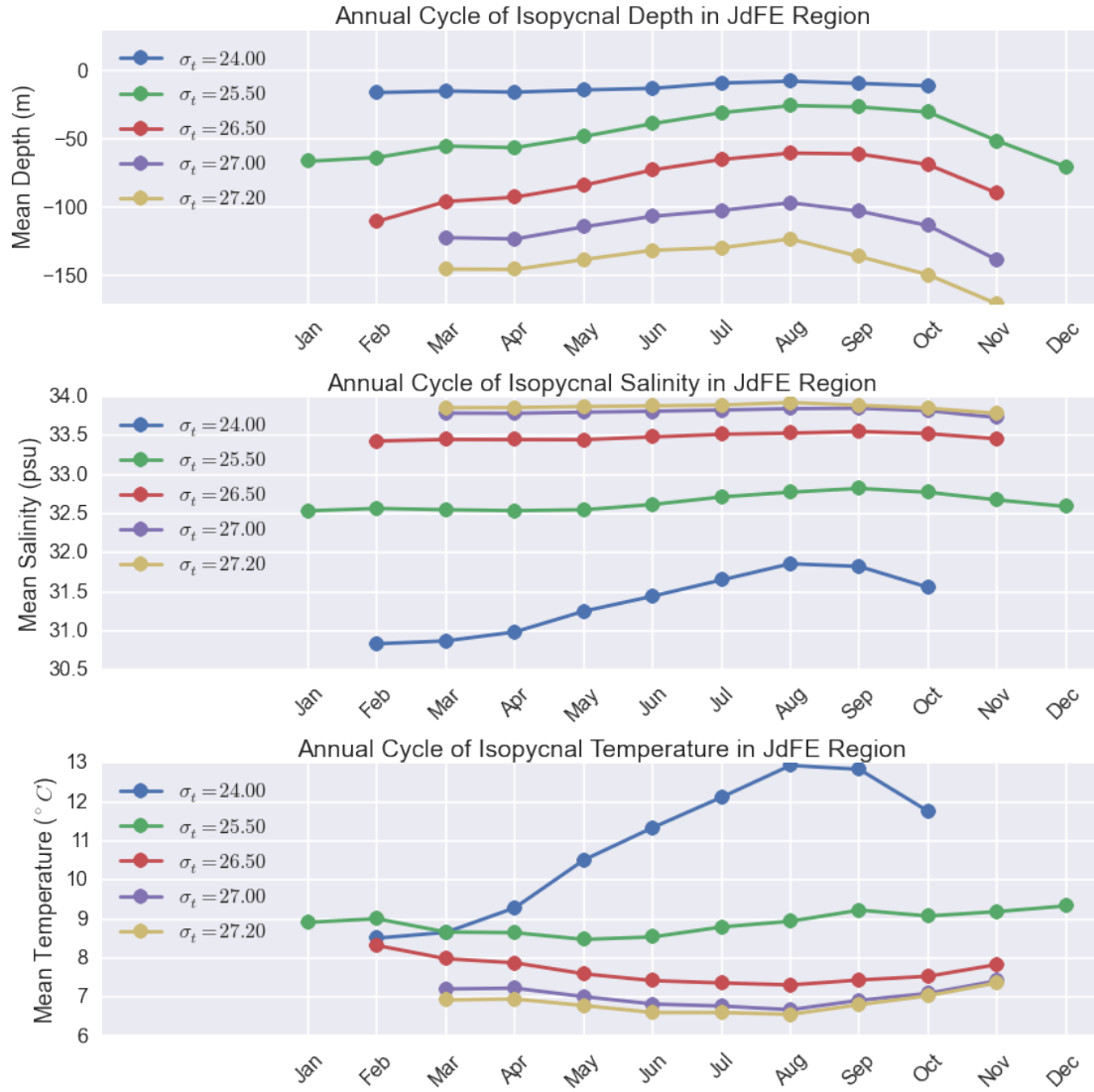
Figure 5.1: The annual isopycnal cycle of: depth, salinity and temperature. Only months with sufficient data (greater than 20 casts with isopycnal data) were kept.
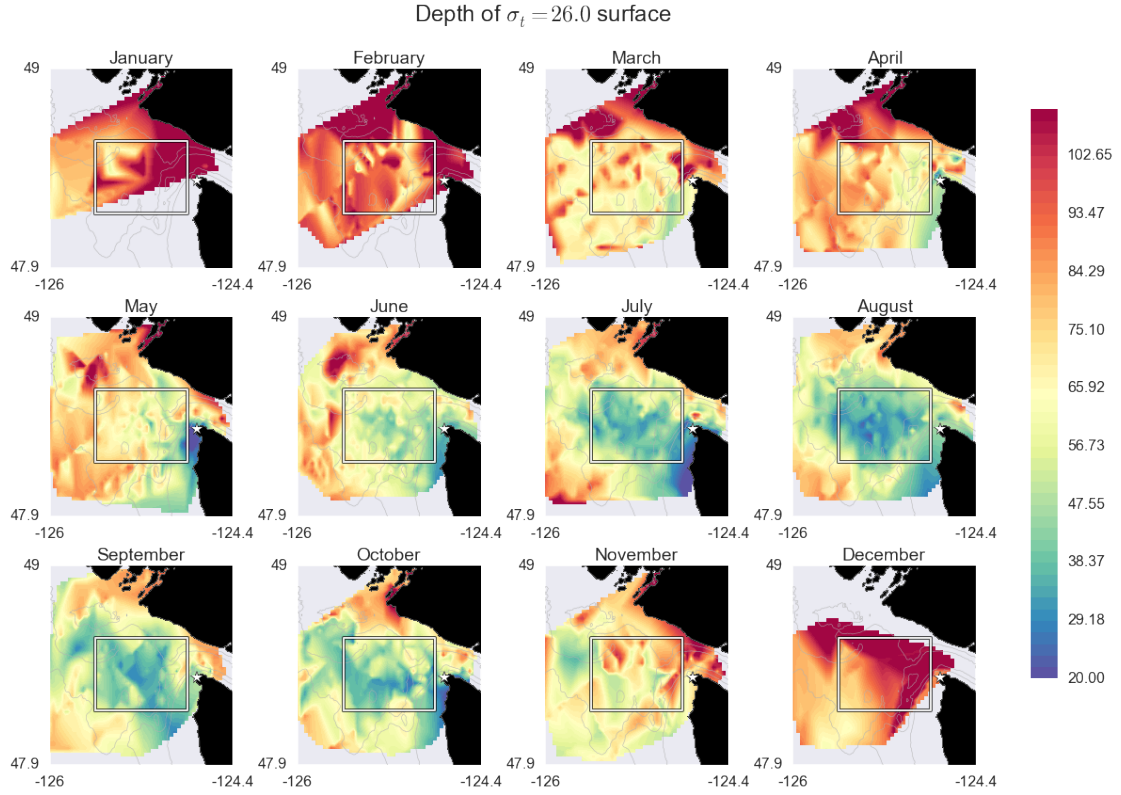
Figure 5.2: The depth of the $\sigma_t = 26.0 kg \cdot m^{-3}$ surface. Note that January, February and December have very little cast information. The white star is Cape Flattery.

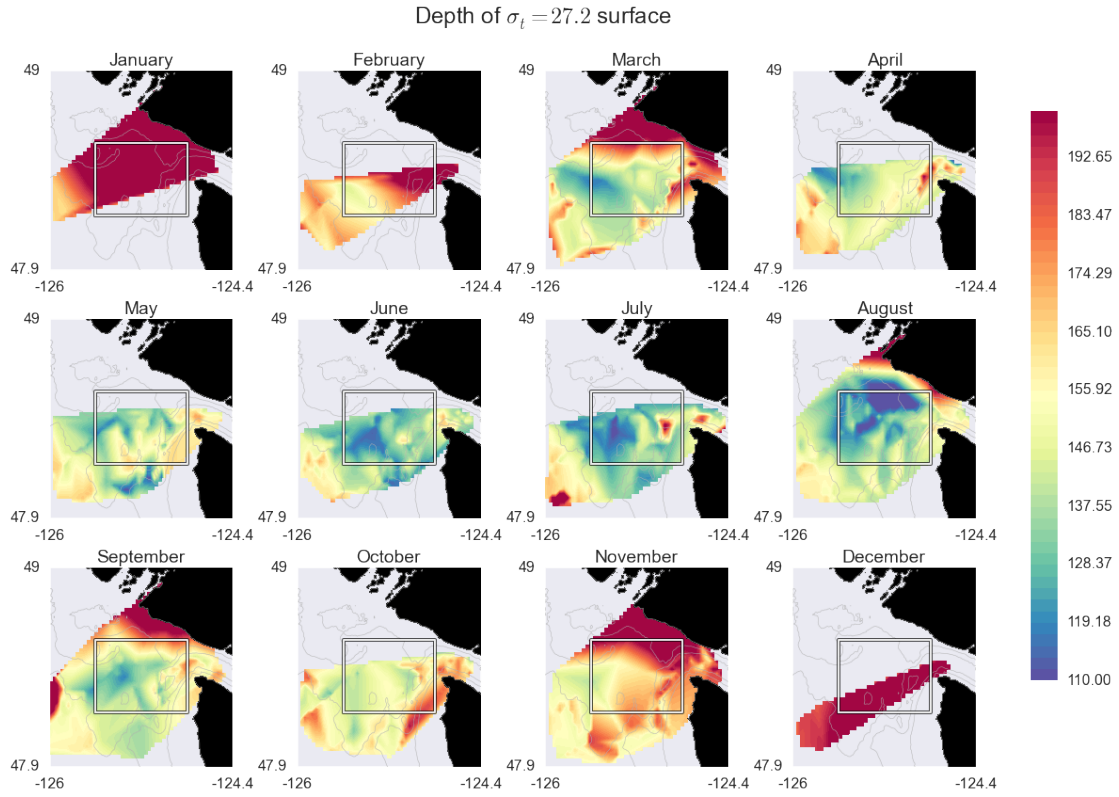Figure 5.3: The depth of the $\sigma_t = 27.2 kg \cdot m^{-3}$ surface. Note that January, February and December have very little cast information.
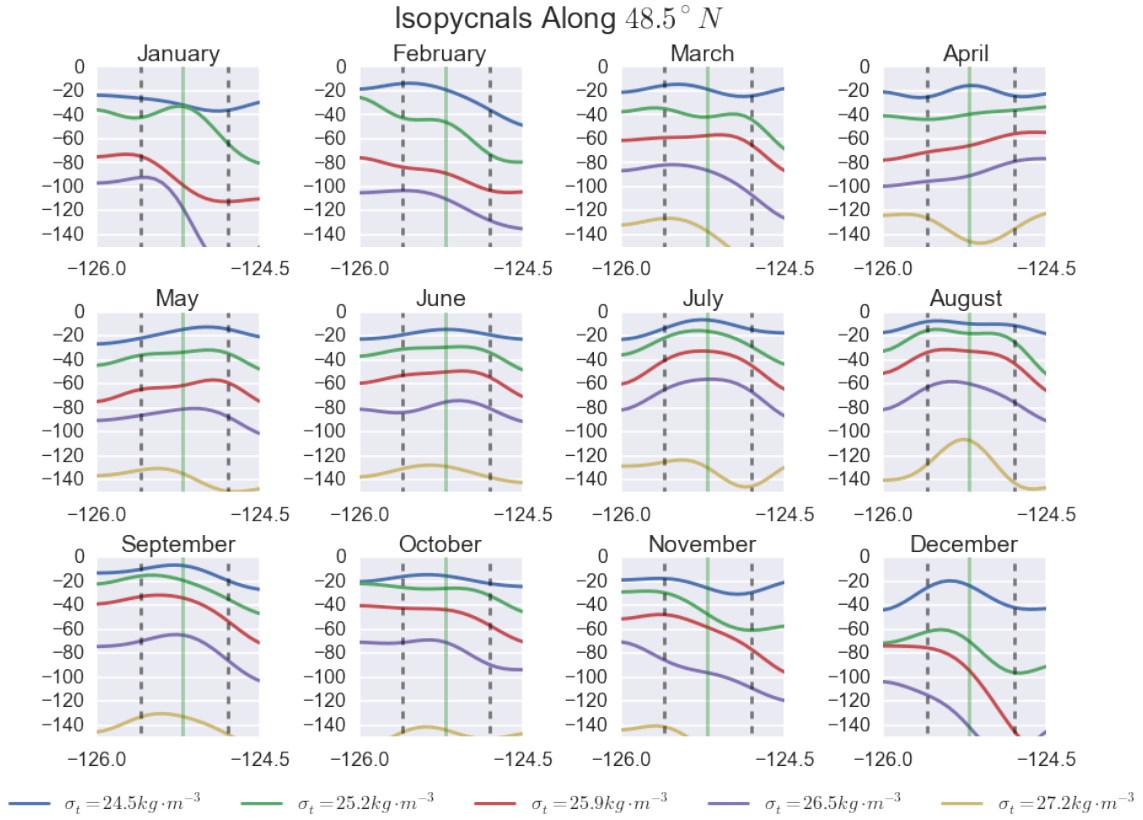
Figure 5.4: Filtered isopycnals in the region around the eddy. Vertical dashed lines denote the "eddy region", while the vertical green line denotes the approximate longitude of Spur Canyon.

# Bibliography

[Bakun, 1975] Bakun, A. (1975). Daily and weekly upwelling indices, west coast of north america. *NOAA Technical Report NMFS SSRF-693*, page 114.

[Crawford and Thomson, 1991] Crawford, W. R. and Thomson, R. E. (1991). Physical oceanography of the western canadian continental shelf. *Continental Shelf Research*, 11(8):669–683.

[Flament, 2002] Flament, P. (2002). A state variable for characterizing water masses and their diffusive stability: spiciness. *Progress in Oceanography*, 54(1):493–501.

[Flather, 1988] Flather, R. A. (1988). A numerical model investigation of tides and diurnal-period continental shelf waves along vancouver island. *Journal of Physical Oceanography*, 18(1):115–139.

[Foreman et al., 2008] Foreman, M., Callendar, W., MacFadyen, A., Hickey, B., Thomson, R., and Di Lorenzo, E. (2008). Modeling the generation of the juan de fuca eddy. *Journal of Geophysical Research: Oceans (1978–2012)*, 113(C3).

[Freeland and Denman, 1982] Freeland, H. and Denman, K. (1982). A topographically controlled upwelling center off southern vancouver island. *Journal of Marine Research*, 40(4):1069–1093.

[Gay and Chereskin, 2009] Gay, P. S. and Chereskin, T. K. (2009). Mean structure and seasonal variability of the poleward undercurrent off southern california. *Journal of Geophysical Research: Oceans (1978–2012)*, 114(C2).

[Hickey, 1979] Hickey, B. M. (1979). The california current systemhypotheses and facts. *Progress in Oceanography*, 8(4):191–279.

[Lynn and Simpson, 1987] Lynn, R. J. and Simpson, J. J. (1987). The california current system: The seasonal variability of its physical characteristics. *Journal of Geophysical Research: Oceans (1978–2012)*, 92(C12):12947–12966.

[Mackas et al., 1987] Mackas, D. L., Denman, K. L., and Bennett, A. F. (1987). Least squares multiple tracer analysis of water mass composition. *Journal of Geophysical Research: Oceans (1978–2012)*, 92(C3):2907–2918.

[Meinvielle and Johnson, 2013] Meinvielle, M. and Johnson, G. C. (2013). Decadal water-property trends in the california undercurrent, with implications for ocean acidification. *Journal of Geophysical Research: Oceans*, 118(12):6687–6703.

[Nelson, 1977] Nelson, C. (1977). Wind stress and wind stress curl over the california current. *NOAA Technical Report NMFS SSRF-714*, page 89.

[Thomson et al., 2007] Thomson, R. E., Mihály, S. F., and Kulikov, E. A. (2007). Estuarine versus transient flow regimes in juan de fuca strait. *Journal of Geophysical Research: Oceans (1978–2012)*, 112(C9).

[Thomson and Ware, 1996] Thomson, R. E. and Ware, D. M. (1996). A current velocity index of ocean variability. *Journal of Geophysical Research: Oceans (1978–2012)*, 101(C6):14297–14310.

[Tully, 1941] Tully, J. P. (1941). Surface non-tidal currents in the approaches to juan de fuca strait. *Journal of the Fisheries Board of Canada*, 5(4):398–409.

[Vindeirinho, 1998] Vindeirinho, C. (1998). *Water properties, currents and zooplankton distribution over a submarine canyon under upwelling-favorable conditions*. PhD thesis, University of British Columbia.